

General Disclaimer

One or more of the Following Statements may affect this Document

- This document has been reproduced from the best copy furnished by the organizational source. It is being released in the interest of making available as much information as possible.
- This document may contain data, which exceeds the sheet parameters. It was furnished in this condition by the organizational source and is the best copy available.
- This document may contain tone-on-tone or color graphs, charts and/or pictures, which have been reproduced in black and white.
- This document is paginated as submitted by the original source.
- Portions of this document are not fully legible due to the historical nature of some of the material. However, it is the best reproduction available from the original submission.



Technical Memorandum 85105

(NASA-TM-85105) SATURN'S OUTER
MAGNETOSPHERE (NASA) 66 p HC A04/MF A01
CSCL 03B

N84-11084

Unclas
G3/91 42275

Saturn's Outer Magnetosphere

A.W. Schardt, K.W. Behannon, J.F. Carbary,
A. Eviatar, R.P. Lepping, and G.L. Siscoe

SEPTEMBER 1983

National Aeronautics and
Space Administration

Goddard Space Flight Center
Greenbelt, Maryland 20771



Saturn

Part III - Magnetosphere
Outer Magnetosphere

A.W. Schardt¹, K.W. Behannon¹, J.F. Carbary², A. Eviatar^{3,4}
R.P. Lepping¹, and G.L. Siscoe³

¹NASA Goddard Space Flight Center
Greenbelt, MD 20771

²Applied Physics Laboratory, John Hopkins Road,
Laurel MD 20811 and
Mission Research Corp., 1720 Randolph Road, SE
Albuquerque, NM 87106

³Dept. of Atmospheric Sciences, University of California
Los Angeles, CA 90024

⁴Permanent address: Dept. of Geophysics and Planetary Sciences
Tel-Aviv University, 69978 Ramat-Aviv, Israel

Abstract

There are many similarities between the Saturnian and terrestrial magnetospheres. Both have a bow shock and magnetopause with a standoff distance that scales with solar wind pressure as $p^{-1/6}$; however, the high-Mach number bow shock is similar to that of Jupiter and differs from the low-Mach shocks of the terrestrial planets. The magnetic field in the outer magnetosphere requires a planetary dipole field, a ring current field, plus contributions from magnetopause and tail currents. Saturn, like Earth, has a fully-developed magnetic tail, 80 to 100 R_S in diameter. Pioneer 11 made multiple crossings of the tail current sheet during its near equatorial outbound trajectory in the dawn direction. One major difference between the two outer magnetospheres is the hydrogen and nitrogen torus produced by Titan which maintains the plasma density between 10^{-2} and 5×10^{-1} ions/cm³ and a temperature of $\sim 10^6$ K. This plasma is, in general, convected in the corotation direction at nearly the rigid corotation speed. Energies of magnetospheric particles extend to above 500 keV. A large increase in the proton and electron population below ~ 500 keV is found at the magnetopause. In contrast, interplanetary protons and ions above 2 MeV have free access to the outer magnetosphere to distances well below the Stormer cutoff. This access presumably occurs through the magnetotail. As a result, the proton energy spectrum has two components: a low-energy power law component, $E^{-\gamma}$, with $\gamma \sim 7$, which becomes less steep below 100 keV; and a much harder interplanetary high-energy component with $\gamma \sim 2$. In addition to the H^+ , H_2^+ , and H_3^+ ions primarily of local origin, energetic He, C, N, and O ions are found with solar composition. Their flux can be substantially enhanced over that of interplanetary ions at energies of 0.2-0.4 MeV/nuc. Proton pitch-angle distributions are generally pancake, while electron pitch-angle distributions may be either dumbbell (field-aligned) or pancake. Field-aligned flow of protons and electrons was observed at various positions in the magnetosphere. Acceleration of particles into the several-hundred-keV range must be taking place in the tail. Besides the field-aligned streaming mentioned earlier, Voyager 2 observed impulsive electron acceleration; and rapid changes in the proton and electron population ($E \sim 1$ MeV) require, at times, the existence of an intense source. No evidence has been found in the magnetotail for either radial outflow of plasma or the presence of a magnetic anomaly at Saturn, but the spectrum of electrons and ions in the magnetotail appears to be modulated by the Kronian period.

Introduction

A planetary magnetosphere is formed by the interaction between the solar wind its embedded magnetic field and the magnetic field near the planet⁽¹⁾. The latter field can be due to ionospheric currents as at Venus or due to the planetary dynamo field as at Earth, Jupiter and Saturn. Various processes in the magnetosphere require energy, such as heating the ambient plasma to a super-thermal temperature, accelerating electron and ions to energies in the MeV range, or creating an aurora. At Earth, the magnetospheric processes derive their power primarily from the solar wind; at Jupiter, the magnetosphere probably extracts most of its energy from the rotational energy of the planet. The Kronian magnetosphere is of special interest because its parameters are intermediate, and both processes might make significant contributions.

The outer magnetosphere and magnetotail are thought to be the primary regions where the solar wind energy is transferred to the magnetosphere; they are also regions where instabilities in the rapidly rotating plasma may be able to extract energy from the planetary angular momentum. To date, we have found good evidence for solar wind effects, but evidence for major rotational energy sources at Saturn is still lacking. Because of the evolution of the solar wind between 1 and 9.5 AU, the details of the interaction at Saturn may be quite different from those at Earth, but the major features such as the existence of a bow shock and magnetopause are unchanged. The density of the solar wind is only 1% of its density near Earth, the Alfvénic-Mach number has

(1) For clarity of presentation we have deleted all references from the summary. References about the magnetosphere of Saturn are given later in the chapter. For more information on The Jovian Magnetosphere the reader should refer to Dessler (1983), and on The terrestrial Magnetosphere to Hess (1968), or any number of other reviews. The changes in the properties of the solar wind are discussed by Smith and Wolfe (1977).

increased substantially, and the density and velocity fluctuations have damped out, while forward and reverse shocks have developed at the boundaries between solar wind streams with appreciable velocity differences.

The outer magnetosphere is generally defined as the region in which the field in the magnetosphere is no longer symmetric around the planet. The solar wind compresses the magnetosphere in the subsolar hemisphere and distends it on the down-stream side where the outer magnetosphere merges gradually into the magnetotail. The energetic particles have soft spectra, and their fluxes show considerable temporal variability. Trapping lifetimes tend to be short, and near the magnetopause particles can probably not complete a drift orbit around the planet. The boundary between the inner and outer magnetosphere is not sharp and covers the range from 5 to 10 R_S at Saturn ($1R_S = 60,330\text{km}$, Saturn's radius). Because the E-ring and Rhea absorption processes fall logically into the discussion of the inner magnetosphere, this chapter covers primarily the region from 10 R_S to the magnetopause and bow shock.

Saturn's outer magnetosphere is filled with thermal plasma with a density of 2×10^{-2} to 5×10^{-1} ions cm^{-3} near the equator. The density decreases at higher latitudes because the scale height is moderately small in the centrifugal potential. No such plasma exists in the outer terrestrial magnetosphere; there are two reasons for the difference. First, Titan is a plasma source in addition to the polar ionosphere. Photo-ionization of neutrals escaping from Titan's atmosphere are the dominant process, and direct interaction between the magnetosphere and Titan's ionosphere is another mechanism when Titan is inside the magnetopause. In addition, plasma is not convected out of the magnetosphere as rapidly as at Earth because the corotational electric field shields the plasma. Continuous readjustments of

the outer magnetosphere to solar wind fluctuations are probably responsible for heating the plasma and producing a tail of superthermal particles. As a result, the energy density in the plasma is often comparable to that of the magnetic field, that is $\beta \sim 1$. Such a plasma can be unstable and may significantly modify the energetic particle population.

The energetic particle population consists of electrons and protons plus some heavier ions. Their energies are mostly less than 2 MeV at 10 R_S and less than 1 MeV near the magnetopause, but higher energy cosmic rays have free access to the outer magnetosphere. On the average, the particle flux increases inward but is subject to large temporal changes. These fluxes and other properties of Saturn's magnetosphere resemble those of the terrestrial magnetosphere which will be used as a point of departure.

The reader should keep in mind that our knowledge about the Kronian magnetosphere is based on data from only three passes through that magnetosphere, those by Pioneer 11 and Voyagers 1 and 2. The relevant instruments on these spacecraft are listed in Table 1. Trajectories together with the bow shock and magnetopause positions are shown in Fig. 1. The three spacecraft entered near the subsolar point at latitudes between 0° and 17° . The spacecraft left the magnetosphere towards dawn, Pioneer 11 and Voyager 2 about -90° from the Saturn-Sun direction and Voyager 1 at about -120° . The latitude of the outbound trajectories was restricted to about $\pm 20^\circ$. We have no direct information about the polar region, the dusk side, or most of the magnetotail. Similarly, we lack data over a large range of interplanetary conditions. Clearly, our understanding of the magnetosphere based on such limited data is bound to contain uncertainties and incorrect interpretation of some of the observations.

The discussion in this chapter has been kept general, but some familiarity on the part of the reader with magnetospheric terminology and phenomena had to be assumed. The motion of trapped charged particles is described by adiabatic theory (e.g. Northrop, 1963; Hess, 1968) which breaks the particle motion down into three components: The motion of the particle around a field line in a gyrocircle, the motion of the center of this circle along the field line and the slow drift around the planet. A constant of the motion, adiabatic invariant, is associated with each of the components. The McIlwain L parameter (McIlwain, 1961) is a convenient way to characterize a drift shell and indicates approximately the distance in R_S at which the particle crosses the equator. In a rotating magnetosphere, a stationary observer sees also the bulk motion of the plasma which may be in rigid or partial corotation (Northrop and Birmingham, 1982). Electric and magnetic field fluctuations permit particles to move radially across magnetic field lines, and because of the random nature of the fluctuations, this process can be described as a diffusion of the particle density (Schulz and Lanzerotti, 1974; Birmingham and Northrop, 1981).

Solar Wind - Magnetosphere Interaction

The interaction of the solar wind with an obstacle like Saturn's magnetosphere can be modeled by gasdynamic theory in which particle collisions in classical theory are replaced by coupling through electric and magnetic field fluctuations in the solar wind (Spreiter et al., 1966, 1968). A detached bow shock forms if the flow is supersonic, and a transition region called the magnetosheath is created in which the shocked solar wind plasma flows around the object. The magnetopause is the boundary between the solar wind plasma and the obstacle or magnetosphere. Because the magnetosphere is not rigid,

the magnetopause occurs at a distance where the momentum flux of the impinging solar wind is balanced by internal pressure at the boundary of the magnetosphere. The "subsolar" distance where this occurs is proportional to the inverse 1/6 power of the solar wind ram pressure if the compressibility of the planetary magnetic dipole field controls the magnetopause position. This is the case at the Earth and was also found to be true at Saturn (Bridge et al., 1981 and 1982; Slavin et al. 1983). In contrast, the relation is $p^{-1/3}$ at Jupiter where the dynamic solar wind pressure is primarily balanced by the pressure and diamagnetic effect of the magnetospheric plasma rather than by the planetary field itself (Siscoe et al., 1980).

A variety of solar wind conditions existed during the Saturn encounters of Pioneer 11 and Voyagers 1, 2. Table 2 lists the positions relative to Saturn at which the bow shock and magnetopause were encountered. These were identified in both the magnetic field and plasma signatures, except for some outbound crossings (especially for Voyager 2) during which the magnetic signatures were less distinct. A fast solar wind stream compressed the magnetosphere just prior to the time when Pioneer entered the magnetosphere at $17.3 R_S$. The solar wind pressure relaxed while Pioneer 11 was in the magnetosphere and must have been quite variable to account for the many outbound crossings of the magnetopause and bow shock. The solar wind conditions were relatively stable during the Voyager 1 encounter and the bow shock and magnetopause were observed at "typical" distances, but the subsolar magnetosheath was significantly thinner than during the other crossings. However, even during this encounter, the dynamic solar wind pressure varied by at least a factor of two (Bridge et al., 1981) as deduced from interplanetary Voyager 2 measurements made at the appropriate time to account for the propagation delay between the two spacecraft.

The Voyager 2 encounter with Saturn occurred during more disturbed interplanetary conditions than the others. An interplanetary shock wave had passed this region 3 1/2 days prior to encounter and an interplanetary current sheet 12 hours after the shock. The magnetic field jumped from < 0.7 nT to > 1.0 nT in the shock, and both the density and speed of the solar wind increased (E.C. Sittler, private communication). Inbound, five bow shock crossings were observed between 31.5 and $23.6 R_S$. Voyager 2 entered a compressed magnetosphere at $18.5 R_S$, but the magnetosphere must have expanded while the spacecraft was in the magnetosphere because the last outbound magnetopause crossing did not occur until $70.4 R_S$ (Table 2). Observations of the dynamic pressure of the solar wind during the preceding nine months gives a $\sim 3\%$ chance, based on the $p^{-1/6}$ scaling, that the magnetosphere could have expanded that much (Behannon et al., 1983; Bridge et al., 1982; Ness et al., 1982). An alternate explanation for the large size is that Saturn passed through the extended Jovian magnetotail (Scarf et al., 1982; Warwick et al., 1982). Prior to the Saturn encounter, recurring anomalous magnetic field, plasma and plasma-wave features observed by Voyager 2 were interpreted as encounters of the Jovian tail at $\sim 9000 R_J$ from Jupiter (Scarf, 1979; Scarf et al., 1981b, 1982; Lepping et al., 1982; Kurth et al., 1982; Desch, 1983), and the geometry for encountering the Jovian tail was still favorable while Voyager 2 was in Saturn's magnetosphere (Behannon et al., 1983).

These differences between encounters were also reflected in the particle population and other properties of the outer magnetosphere and will be discussed in the next sections. The observed large changes of the boundary location introduce uncertainties into the deduced shape of the bow shock and magnetopause. The shapes appear to be similar to those in the terrestrial magnetosphere, but the bow shock and magnetopause at Saturn may be somewhat

blunter in ecliptic plane projection (Slavin et al., 1983; Smith et al., 1980). Observations were made only near the equatorial plane of Saturn, and no definitive information is available about the shape in a meridional plane.

The solar wind-magnetosphere interaction at Saturn occurs at sonic- and Alfvénic-Mach numbers of 10-20 and at pressures that are down by a factor of ~ 100 from those at Earth. A major effect of the higher Mach number, as predicted by gas dynamic theory, is a larger jump in the plasma temperature across the shock, which should be proportional to the square of the Mach number (Spreiter et al., 1966). This increase was observed in the jump of electron temperatures $T_e^{(2)}/T_e^{(1)}$ which is ~ 50 at Saturn, ~ 15 at Jupiter, and only 3-4 at Earth (Scudder et al., 1981; Scudder, private communications). Plasma-wave turbulence was observed at the Saturnian bow shock, which suggests that the plasma instabilities associated with the higher Mach number shock differ from those of lower Mach numbers found at the terrestrial planets (Scarf et al., 1981a). The enhancement of the wave spectrum below the ion plasma frequency characteristic of bow shocks at Earth and Venus is not observed at Jupiter or Saturn.

In the subsolar hemisphere, the Saturnian bow shock is a strong, quasi-perpendicular shock, as is to be expected from the average spiral angle direction of the interplanetary field. Thus, the field magnitude changes at the shock but not its direction (Fig. 2). The jump in magnitude is significantly sharper when the magnetosphere contracts than when it expands (Lepping et al., 1981a; Smith et al., 1980). The shock is about 2000 km thick corresponding to a few ion inertial lengths, much smaller than the ion cyclotron radius and larger than the electron cyclotron radius. Thus, cyclotron waves do not play a major role in the formation of the shock.

The level of plasma waves in the magnetosheath was found to be extremely low (Scarf et al., 1981a). At much lower frequencies, the magnetic field magnitude varied semi-periodically throughout the sheath (Fig. 2) during the Pioneer 11 and Voyager 1 inbound passes. These large field changes are anti-correlated with the plasma density in the sheath. Lepping et al. (1981a) have interpreted these observations in terms of slow mode magnetosonic waves. An alternate explanation is based on the Zwan and Wolf (1976) mechanism. The large size and bluntness of the magnetopause may mean that flux tubes remain in the sheath for a relatively long time and the plasma could drain off by moving parallel to the field (Slavin et al., 1983; Smith et al., 1980). In this explanation, an unspecified wave is required to account for the even spacing throughout the sheath. No such fluctuations in field magnitude were observed by Voyager 2 during its inbound magnetosheath passage.

The magnetopause of Saturn as well as that of the other planets may generally be characterized by a tangential discontinuity in the magnetic field. A minimum variance analysis applicable to tangential discontinuities (Siscoe et al., 1968) and the more general method of Sonnerup and Cahill (1967) give consistent results. These analyses give the direction of the normal to the magnetopause, and the directions agree with those predicted by the models of the magnetopause position (Lepping et al., 1981a; Ness et al., 1982; Smith et al., 1980). The presence of surface waves on the magnetopause was deduced from the five regularly spaced crossings during the Voyager 1 inbound pass (Figs. 2 and 3). Such waves have also been seen at the Earth's magnetopause and were studied initially by Aubry et al. (1971; see also Lepping and Burbaga, 1979 and references therein). The waves at Saturn may be characterized by a period of 23m, an amplitude of $\sim 0.5 R_S$, and a wave length of $\sim 5 R_S$. It is believed that they propagate parallel to the equatorial

plane of Saturn and "tailward" with a velocity of 180 ± 90 km/s (Lepping et al., 1981a). These characteristics are consistent with a Kelvin-Helmholtz instability operating at the frontside of the magnetopause which is driven by the faster moving plasma in the magnetosphere. This is in contrast to the case at Earth, where the waves at the dawn and dusk magnetopause are thought to be driven by the more rapidly moving magnetosheath plasma (Miura and Pritchett, 1982; Pu and Kivelson, 1983).

The magnetopause constitutes a boundary to electrons, protons, and ions with energies below 0.5 MeV. An exception to this rule occurred during the Voyager 2 inbound pass when enhanced energetic particle fluxes were already observed 15 minutes prior to the magnetopause crossing as identified by magnetometer and plasma cup data (Krimigis et al., 1982; Voigt et al., 1982). This increase was accompanied by a change in the magnetic field of the magnetosheath from one with a vertical component opposite to the planetary field to one with a parallel vertical component. The first order anisotropy in the angular distribution of protons suggests that the magnetopause was moving inward at that time with a speed of 10 km s^{-1} . The enhanced density of hot plasma in the outer magnetosphere may have changed the magnetopause characteristics during the Voyager 2 observations (MacLennan et al., 1983).

The Cold Plasma in the Outer Magnetosphere

The plasma density decreases at the magnetopause and its temperature increases (Fig. 4) as the spacecraft moves from the sheath into the hotter magnetospheric plasma (Bridge et al., 1981). At the Earth, in contrast, no thermal plasma is found between $\sim 5.6 R_E$ and the magnetopause. Before discussing the variations of the plasma parameters, let us first treat the average properties of the thermal plasma in the outer magnetosphere. A syn-

thesis of the data from the three spacecraft shows a fairly thick sheet of plasma with a radial density profile proportional to $L^{-3.5 \pm 0.5}$ (Fig. 5). An ion spectrum taken about $0.5 r_S$ south of the equator at $L \approx 15$ (Fig. 6) shows a heavy ion component of either O^+ or N^+ which has three times the number density of protons (Bridge et al., 1981). In the centrifugal potential of a rotating magnetosphere, the heavy ions should dominate at the center of the sheet because of ambipolarity. This effect is demonstrated by comparing ion spectra taken at different latitudes (Fig. 7). The Voyager 2 spectra taken at 18° contain almost no heavy ions. It may also be noted from Fig. 7 that the temperature of the hydrogen component was considerably higher during the Voyager 2 encounter (the distribution function peaked at a higher energy and was wider). In a two component plasma, a higher temperature of the light component would be expected off the equator, but differences in the state of the magnetosphere may also have contributed to the difference between the two passes.

One major difference between the outer magnetospheres of Saturn and Earth is the presence of the giant satellite Titan and its dense atmosphere. At any given time Titan can be in the magnetosphere, in the magnetosheath, or in the solar wind (Wolf and Neubauer, 1982). The statistics of magnetopause locations given by Siscoe (1978) when extrapolated to the observed magnetic moment of Saturn lead to the prediction that the orbit of Titan will lie wholly within the magnetosphere approximately 50% of the time. In fact, of the three spacecraft that have flown past Saturn, only Voyager 1 found Titan's entire orbit enclosed within the magnetosphere. Titan itself, however, is generally inside the magnetosphere because it spends relatively little time near the subsolar part of its orbit.

Titan, its atmosphere, and the Titan-magnetosphere interaction are dealt

with elsewhere. Our interest in Titan is restricted to its role as a source of plasma. Titan is the direct source of a stream of plasma extending in the local corotation direction. Estimates of the source strength range from 1.2×10^{24} ions/sec (Gurnett et al., 1982) to 6×10^{24} ions/sec (Bridge et al., 1981). This matter is apparently made up primarily of heavy ions of mass 14 (N^+) and possibly even molecular ions of mass 28 (N_2^+ or H_2CN^+) (Hartle et al., 1982). This directly outflowing plasma or Titan plume tends to remain in the equatorial plane and to merge into the background, somewhat as a comet tail eventually merges into the interplanetary plasma.

In addition to the stream in the Titan wake (density peak no. 1 in Fig. 4), the PLS instrument on Voyager 1 also encountered density enhancements inward and outward of the orbit of Titan (density peaks 2, 3 and 4 in Fig. 4). These enhancements are also characterized by a high density and a low temperature and have been interpreted by Eviatar et al. (1982) to be multiple encounters with the extended Titan plume. They showed that the plume would be wrapped around Saturn by corotation and could last three Kronian periods before being reduced to the density of the background plasma. The plume would be dispersed by the combined effects of acceleration up to corotation speed, of radial expansion by the centrifugal interchange mode and of heating which increases the vertical thickness of the plume. The radial displacements of the plume as a whole are related to magnetopause motions driven by variations in solar wind dynamic pressure. In addition to the density enhancements tentatively identified as the extended plume of Titan, other less pronounced enhancements occur between $L = 10$ and 17 (Fig. 4) which are also correlated with lower temperatures. At a higher latitude of $\sim 18^\circ$, Voyager 2 observed similar density increases but these correlate with higher rather than lower temperatures. It has been suggested that the flux tube content remains

constant and that the decrease in scale height at lower temperatures concentrates the plasma near the equator (Sittler et al., 1983). This can account for the anti-correlation between temperature and density near the equator and correlation at a higher latitude.

An alternate explanation for the large variation of the plasma density in the outer magnetosphere has been proposed by Goertz (1983). The plasma becomes potentially unstable against radial outflow when the centrifugal force on the plasma exceeds the magnetic field stress; this occurs when the corotation energy density of the plasma becomes greater than the magnetic field energy density (Hill et al., 1974; Kennel and Coroniti, 1978). This condition is satisfied at some locations in the outer magnetosphere. For instance at L=15 near the equator, Bridge et al., (1981) find a heavy ion plasma rotating at 139 km s^{-1} with a density of $\sim 0.4 \text{ cm}^{-3}$. Since the magnetic field is about 10nT, the corotation energy density is about twice the field energy density for a nitrogen plasma. The solar wind pressure would inhibit radial outflow in the subsolar hemisphere, but plasma outflow into the tail will occur if the instability can grow sufficiently rapidly. In contrast to Evitar et al. (1982), Goertz (1983) concluded that the Titan plume and the high density edge of the plasma sheet at L~15 (Fig. 4) are sufficiently unstable to produce radial outflow into the magnetotail in the form of a planetary wind. In this picture, detached plasma blobs from the inner, stably-trapped plasma sheet account for most of the density enhancements observed by Voyagers 1 and 2.

The plasma in the outer magnetosphere may also be moved around by means of a large-scale magnetospheric circulation, which is referred to as convection. In the case of Earth, the solar wind exerts a tangential drag on the magnetospheric plasma near the magnetopause. A convection pattern results

which is fixed in the frame of reference in which the magnetopause is at rest. The depth of penetration of the convection into the magnetosphere is limited by a tendency of the resident plasma to corotate with the planet. The tendency to corotate increases toward the planet. In the case of the Earth, the convection pattern penetrates about half way from the magnetopause to the Earth. Locally generated plasma in this region is, in a manner of speaking, scoured out by the convection. Brice and Ioannides (1970) predicted on the basis of a simple scaling argument that at Jupiter rotation should dominate over convection all the way to the magnetopause. The same conclusion should also apply to Saturn (Scarf, 1975); however, Kennel and Coroniti (1978) pointed out that the Brice and Ioannides calculation ignored the time dependence of the convection process, and this could occasionally expose the outer magnetosphere to convective transport. The possibility is more likely in the case of Saturn where rotational dominance is predicted to be smaller than at Jupiter. Since the refill time scale can be very long in the large volume of the Saturnian magnetosphere, the scars left by occasional scouring events would persist for a correspondingly long time (Siscoe, 1979). It is possible that the discontinuity in the radial density profile between $L = 8$ and $L = 9$ seen in the Pioneer 11 data in Fig. 5 is such a scar. A more definitive test for the presence of the scouring process was possible with the Voyager data, which permitted a determination of the radial profile of the total number of electrons contained in a unit magnetic flux tube. In contrast to the number density profile, the magnetic flux tube content showed no appreciable discontinuity in the outer magnetosphere at least out to $L = 14$ (Bridge et al., 1982), but almost complete plasma dropouts were observed beyond $L = 14$ (Fig. 4). We may infer that rotation completely dominates solar wind driven convection to this distance.

The above discussion has shown that several processes individually or in combination can account for the large fluctuations in plasma density observed outside of L=15. On a phenomenological basis, this region has been described as the plasma mantle, and we find that magnetic field magnitudes and the fluxes of more energetic particles (Krimigis et al., 1982) also show larger temporal variations in this region than inside of L ~ 15.

In addition to the plume of Titan, there are several other candidate sources for the observed plasma. Ionization of the large neutral cloud of hydrogen reported by the UVS group (Broadfoot et al., 1981) will be a much stronger source of plasma than the Titan plume. Bridge et al. (1982) calculated the neutral hydrogen lifetime against ionization processes and found a maximum lifetime near Titan where photoionization is the dominant process. Closer to Saturn the plasma density increases, and the hydrogen is lost to both charge exchange and electron impact ionization. In equilibrium, the rate at which plasma is generated from the neutral cloud must be equal to the rate at which the neutral hydrogen is added to the cloud by nonthermal escape from Titan, which occurs at the rate of approximately 2×10^{26} atoms s^{-1} . Also according to their calculation, nonthermal escape of atomic nitrogen occurs at the rate of approximately 3×10^{26} atoms s^{-1} . Under the assumption that all of the neutral matter entering the cloud is ionized, mass is added to the plasma from all of the Titan-related sources at a rate of the order of $7 \text{ kg } s^{-1}$. Protons could also originate from the atmosphere of Saturn, and both protons and oxygen ions would be produced by sputtering of the icy satellites, Tethys, Dione and Rhea (Lanzerotti et al., 1983b) and of the A ring. Thus, the composition at any one point is determined by the relative source strength, by possible loss mechanisms, and by transport that redistributes ions once they are formed.

In addition to the rapid transport mechanisms described above, a more uniform redistribution of the plasma can be achieved by means of diffusion. Diffusion can be driven by the centrifugal force (autotropic diffusion; Siscoe and Summers, 1981) or by the electric field generated in the dynamo region of the atmosphere and mapped into the magnetosphere along the highly conducting magnetic field lines (heterotropic diffusion; Brice and Ioannidis, 1970). In the Jovian magnetosphere, the Io torus provides a large mass on which the centrifugal force can act, thereby assuring the dominance of autotropic over heterotropic diffusion. At Saturn, on the other hand, the mass of locally generated plasma is much smaller, and it is not evident which mode of diffusion dominates. However, as Siscoe and Summers (1981) showed for Jupiter's magnetosphere, the radial density profile produced by the two types of diffusion are virtually indistinguishable. Both yield profiles of the form L^{-p} where p depends on precise details of the structure of the turbulence either in atmosphere or in the magnetosphere. A value between 3 and 4 is consistent with predictions based on simple models of the driving turbulence in both cases.

For heterotropic diffusion, the applicable diffusion coefficient has the paradigmatic form

$$D = kL^3 \quad (1)$$

where $k = 1 \times 10^{-10} R_J^2 \text{ sec}^{-1}$ has been suggested by extrapolation from Jupiter (Siscoe, 1979). Krimigis et al. (1981) have derived a diffusion coefficient from electron observations near Rhea with $k \sim 6 \times 10^{-11} R_J^2 \text{ sec}^{-1}$. A steady state model of the population of the region by neutral and ionized matter from Titan yields a similar value for the diffusion coefficient (Eviatar and Podolak, 1983). These results are consistent with radial transport by means

of simple heterotropic diffusion, but they do not constitute a definitive determination of the transport process. Based on the above diffusion coefficient, one can calculate the rate of outward transport of oxygen ions from the inner magnetosphere and balance this against the loss rate due to charge exchange in the neutral hydrogen torus from Titan. This is a very efficient loss mechanism for O^+ ions because of the near resonance of the reaction, and Eviatar et al. (1983) concluded that most of the O^+ ions could not diffuse far beyond the inner boundary ($8 R_S$) of the hydrogen torus.

We have not considered diffusion associated with solar wind fluctuations which can cause motion of the magnetopause and thereby violate the third adiabatic invariant. Such fluctuations are the prime source of radial diffusion of energetic particles in the Earth's magnetosphere

(Fälthammer, 1968) and produce magnetic impulses which generate a diffusion coefficient that varies as L^{10} (Schulz and Lanzerotti, 1974). If the diffusion reported by Krimigis et al., (1981) was attributed to such a process, we would find $k \sim 1.4 \times 10^{-17} R_S^2 s^{-1}$. Averaging this L dependence over the outer magnetosphere gives a mean radial transport rate three orders of magnitude greater than that calculated by Eviatar and Podolak (1983) and would require a cold plasma source strength vastly in excess of the fluxes observed during the Titan encounter (Hartle et al., 1982). It appears therefore that Saturn's outer magnetosphere resembles in this respect more the Jovian than terrestrial magnetosphere.

Another potential plasma source for the outer magnetosphere are the gas and ions surrounding the A ring. A hydrogen cloud of 5×10^{33} atoms has been detected (Broadfoot et al., 1981). A charge exchange reaction between ions corotating with the planet and the neutral cloud would produce energetic neutrals with enough velocity to reach the outer magnetosphere but less than

the local escape velocity. As Eviatar et al. (1983) have shown, these neutrals have a high probability of being re-ionized in the outer magnetosphere and may add significantly to plasma from Titan.

It is of interest to determine whether the plasma in Saturn's outer magnetosphere can corotate with Saturn. For the purpose of this calculation we will ignore the other plasma sources and use only the $\sim 7 \text{ kg s}^{-1}$ of plasma originating directly or indirectly from Titan. Corotation is retarded in Jupiter's magnetosphere by the outflow of plasma composed of matter originating on Io (McNutt et al., 1981). The breaking results from the necessity to supply angular momentum to the outflowing matter by means of an electrical current system that links the magnetospheric plasma to the planet's ionosphere (Hill, 1980). Beyond $20 R_S$, the electrical circuit at Jupiter is no longer able to transfer the angular momentum required to maintain rigid corotation.

The neutral particle torus of Titan produces ions over a large radial range ($6.5\text{--}23.5 R_S$). Because we do not know the mass loading rate as a function of distance, we cannot derive rigorously the partial corotation velocity as a function of distance. However, we can estimate an average by treating the torus as a rigid unit. The resulting expression for the lag is (Eviatar et al., 1983)

$$\frac{V}{V_C} = \frac{\dot{M}_C}{\dot{M}_C + \dot{M}} \quad (2)$$

in which

$$\dot{M}_C \equiv \frac{8\pi \Sigma B_S^2 R_S^2 \Delta L}{c^2 L^5} \quad (\text{in Gaussian units}) \quad (3)$$

where V is the partial corotation speed, V_C , the rigid corotation speed is evaluated at the center of the torus, L ; Σ is the ionospheric height integrated Pederson conductivity, B_S is the equatorial surface magnetic field strength, R_S is the planet's radius, ΔL is the radial thickness of the torus in units of R_S , and \dot{M} is the mass loading rate. Eviatar et al. (1982) have calculated a conductance of $\Sigma = 1.7 \times 10^{10} \text{ cm s}^{-1}$ (or 0.018 mho) on the basis of electron and neutral particle densities in Saturn's ionosphere provided by Voyager data. For $\Delta L = 17$ and $L = 15$, which are representative of the neutral hydrogen torus (Broadfoot et al., 1981), we obtain $\dot{M}_C \sim 14 \text{ kg s}^{-1}$. Another recent estimate (Connerney et al., 1983) of $\Sigma \sim 9 \times 10^{10} \text{ cm s}^{-1}$ gives $\dot{M}_C \sim 70 \text{ kg s}^{-1}$. Using the value of $\dot{M} \sim 7 \text{ kg s}^{-1}$ deduced earlier, we obtain $V/V_C = 0.67 - 0.91$. Bridge et al. (1981) found that corotation was maintained to within 10 percent out to $15 R_S$, but probably began to lag between 15 and $18 R_S$. Given the uncertainties in the determinations of Σ and \dot{M} , we can only conclude that rigid corotation is marginal, and substantial departures may occur at times as seen by Frank et al. (1980).

The Magnetic Field and Hot Plasma in the Outer Magnetosphere

The magnetic field configuration at Saturn resembles that found in the outer terrestrial magnetosphere except that the direction of the field is reversed (Fig. 8 and 9). In the subsolar hemisphere the observed field is higher than the model field because of compression by the solar wind, and in the dawn direction we can observe the onset of the magnetotail (Fig. 8) which will be discussed in a later section (Ness et al., 1981 and 1982; Smith et al., 1980). Fig. 9 shows averaged vector fields for both Voyagers projected into $X_{SM}-Z_{SM}$ plane of the solar-magnetospheric coordinate system (X_{SM} toward

the sun, Z_{SM} positive northward and oriented such that the planetary dipole axis lies in the X_{SM} - Z_{SM} plane; Ness, 1965). The field magnitudes are scaled logarithmically, and the positions of a model magnetopause in the X_{SM} - Z_{SM} plane are illustrated for both missions. The magnetic field observed by Voyager 1 outside of $15 R_S$ pointed almost perfectly southward, which is consistent with the relatively quiet conditions of the solar wind during the early part of the encounter.

Voyager 2 encountered a more compressed magnetosphere, and the hourly averages shown in Fig. 9 were less steady. Initially, the field pointed predominantly southward ($B_z = -6.6$ nT) but with substantial sunward (2.5 nT) and eastward (1.8 nT) components. Starting near $15 R_S$, the field rotated towards the radial direction with a decrease in the eastward component and corresponding increase in the sunward component until B_x was comparable to B_z (at $\sim 10 R_S$ in Fig. 9). These changes have been interpreted in terms of an expansion of the magnetosphere in response to a major decrease of the external pressure (Ness et al., 1982). Based on the position of the magnetopause crossing observed during the outbound pass, such an expansion must have occurred while Voyager 2 was in the magnetosphere, and the field changes identify the time when the expansion occurred. It is quite possible that this expansion occurred because the distant Jovian magnetotail engulfed Saturn at that time (Desch, 1983). Significant changes in the energetic particle population were observed concurrently with the field changes. Their flux became more variable and increased by an order of magnitude followed by a brief decrease by a factor of ~ 40 at $15.5 R_S$ (Vogt et al., 1982). The Voyager 2 observations are at least qualitatively similar to changes in the magnetic field magnitude and direction observed with Pioneer 11 which occurred most likely in response to a large decrease of the solar wind pressure (Smith et al., 1980).

As can be seen in Fig. 8, the addition of a ring current field to the intrinsic planetary magnetic field improves substantially the fit between observations and the model field (Connerney et al., 1981, 1983; Ness et al., 1982). A good fit to both Voyager 1 and 2 data has been obtained with a ring current between $L=8$ and $15.5 R_S$, which falls off as L^{-1} and is confined to within $\pm 3 R_S$ of the equator. Under the assumption of a very cold plasma, Connerney et al. (1983) have derived the ion density in the outer magnetosphere (Fig. 5). Their values are in reasonable agreement with observations but consistently higher. The agreement between observed ion densities and densities derived from the model magnetosphere could be further improved by including the effect of the hot plasma.

The importance of the hot plasma is best expressed in terms of the ratio between the plasma and magnetic field pressures or energy densities. As Krimigis et al. (1983) have shown, this ratio in the outer magnetosphere near the equator is generally between 0.1 and 1.0 (The inbound pass in Fig. 10). When $\beta \sim 1$, the plasma is responsible for a major part of the pressure and can therefore significantly effect the field configuration. The plasma pressure is particularly high at the subsolar magnetopause with $\beta \sim 1$ and thus contributes half of the internal pressure required to balance the dynamic pressure of the solar wind (Smith et al., 1980). A very similar situation exists at the magnetopause of Jupiter (Lanzerotti et al., 1983). Thus one might expect that the magnetopause and bow shock distances would also scale as at Jupiter which is $\propto p^{-1/3}$ rather than as at Earth, $\propto p^{-1/6}$. However, the significant quantity that controls the scaling is not the value of β but the origin of the magnetic field at the magnetopause. At Saturn this field is apparently due to the intrinsic planetary field and thus the magnetopause distance follows the scaling law of a dipole. At Jupiter when the subsolar

magnetopause is beyond $50 R_J$, the field in the outer magnetosphere is highly variable and apparently is primarily due to the magnetospheric plasma/current system. Because the plasma/currents will readjust themselves in response to changes of the solar-wind pressure, a different scaling law applies.

Energetic Particles in the Outer Magnetosphere

A flux of energetic electrons, protons, and heavier ions with energies up to ~ 1 MeV is trapped by the magnetic field of the outer magnetosphere. Fig. 11 gives a three dimensional overview of the ion (protons and heavier ions) and electron spectra observed with Voyager 2. A sharp increase in particle flux occurred at the magnetopause with the largest increase at lower energies. On the average, the flux increased further between the magnetopause and $10 R_S$, although substantial spatial and/or temporal fluctuations were superimposed on the average increase. The most noticeable of these is the decrease in the low energy ion flux inside of $15 R_S$ which coincides with the magnetic field changes discussed previously and is presumably due to an expansion of the magnetosphere in response to a large decrease of the external pressure.

The observed fluxes are not symmetric between the inbound and outbound pass of Voyager 2. This asymmetry is partially due to the difference in latitude but also reflects to a large extent the asymmetry of the magnetosphere between the subsolar direction and the dawn direction (Fig. 1b). The onset of the magnetotail in the dawn direction is reflected in the more rapid decrease of particle flux with distance. These differences will be discussed in the next section on the magnetotail.

During the inbound pass of Voyager 1, the Kronian magnetosphere was less disturbed than during the Pioneer 11 and Voyager 2 encounters; therefore, our

discussion is based primarily on Voyager 1 data with a mention of major differences relative to the other passes. Fig. 12 shows the energetic electron intensities observed at different energies. Large variations are superimposed on the general decrease of the flux with distance from Saturn. These changes are most probably temporal and appear at the same time at all energies. They are thought to reflect the response of the magnetosphere to changing interplanetary conditions; however, other processes may have contributed. For instance, a flux minimum was found at the distance of Titan during both inbound and outbound passes. If the energetic particles constitute the non-Maxwellian tail of the thermal plasma, then the lower temperature in the Titan plume (Fig. 4) could be reflected in a lower flux of energetic particles. The two orders of magnitude flux dropout between 10 and 15 R_S observed outbound will be discussed in the next section. The energetic particle population was relatively stable during the Pioneer 11 pass (Fig. 12b); but large temporal changes were also observed by Voyager 2 especially during the period when the magnetosphere expanded.

The differential energy spectra of electrons in the outer magnetosphere follow a power law in energy, $E^{-\gamma}$, with $\gamma = 3.8$ to 4 during the Pioneer 11 pass (McDonald et al., 1980; Van Allen et al., 1980); γ was in the range from 3.4 to 4 during the Voyager encounters (Krimigis et al., 1983). Such a spectrum is characteristic of magnetospheric electrons and is consistent with a non-Maxwellian tail of a thermal plasma produced by various acceleration processes.

During the Pioneer 11 encounter, the angular distributions of electrons above 0.4 MeV in the outer magnetosphere were field-aligned or "dumbbell" (Fig. 13) near the magnetopause and slowly changed towards "pancake" (perpendicular to the field) distributions at 10 R_S (Bastian et al., 1980;

Fillius et al., 1980; Krimigis et al., 1981, 1982; McDonald et al., 1980; Van Allen et al., 1980). This change in the pitch-angle distribution is illustrated in Fig. 14, where the coefficient of the $\cos 2\theta$ term in the Fourier expansion is plotted versus distances (θ is the angle between the look direction and the projection of the field into the scan plane). Because of the symmetry of particle motion around field lines, this term corresponds to a pitch-angle distribution that is either field-aligned or perpendicular to the field. The distribution is proportional to $1 + b \sin^2\theta$ where $b = 2A_2/(1-A_2)$ and A_2 is negative for dumbbell distributions. The behaviour of the 0.16 to 0.43 MeV channel (Fig. 14) is markedly different from that at higher energies, and the angular distribution changes back and forth between pancake and dumbbell distributions. At yet lower energies, 37-70 keV, the pitch-angle distribution is pancake (Voyager 1) throughout the outer magnetosphere (Krimigis et al., 1983) and changes to dumbbell near Rhea where particles with pitch angles near 90° are preferentially absorbed.

The energy dependent changes in the pitch-angle distribution are probably due to wave-particle interactions. Waves that could be responsible for these pitch-angle changes have not been observed directly, but bursts of electrostatic waves near the electron plasma frequency occur throughout the outer magnetosphere (Fig. 15; Kurth et al., 1982). These bursts resemble terrestrial emissions which are associated with chorus emissions, and the latter do couple to ~ 0.1 MeV electrons.

Butterfly pitch-angle distributions (maximum flux near $\theta = 45$ and 135°) were observed at least at some energies near the inner boundary of the outer magnetosphere at $\sim 10 R_S$ (Fig. 13; the 0.43-0.80 MeV channel at $11.6 R_S$ inbound and the 0.80-1.1 MeV Channel at $9.1 R_S$ outbound). Such distributions can be produced by shell splitting (Roederer, 1967) which occurs if the

trapping field deviates from a dipole field and is asymmetric relative to the subsolar direction. In such a field the drift shells of particles with different mirror points separate as the particles drift around the planet. As a result one can find regions in which the particle population is deficient at certain pitch angles. Based on the asymmetry of the observed magnetic field, shell splitting must occur, but it has not yet been demonstrated that the observed butterfly distributions are due to shell splitting rather than another cause.

Proton fluxes are plotted in Fig. 16. Protons were identified above 2 MeV by the $\Delta E - E$ technique (Stone et al., 1977), but the lower energy channels include contributions from heavier ions; however, composition measurements to be discussed later indicate that the heavy ion contribution is small. Outside the orbit of Rhea and below 1 MeV, the same general trend and temporal variations are present as in the electron flux. Above 2 MeV, the proton flux is unaffected by the presence of the magnetopause and remains at interplanetary values. This effect is clearly visible in the proton energy spectrum (Fig. 17) which consists of two components. The high energy component is due to cosmic rays which gain access to the outer magnetosphere (Vogt et al., 1981). This component was much more intense during the Pioneer 11 encounter when a solar cosmic ray event was in progress and the observed proton to alpha particles ratio was characteristic of cosmic rays (McDonald et al., 1980; Simpson et al., 1980). Because the magnetic field near the magnetopause was undergoing time dependent changes, Simpson et al. (1980) suggested direct penetration of the magnetopause by > 0.5 MeV ions and subsequent trapping. McDonald et al. (1980) suggested that these particles gain access through the magnetotail and then drift into the subsolar hemisphere without being stably trapped; such access occurs in the terrestrial

magnetosphere.

The low energy part of the proton spectrum resembles a hot, convected Maxwellian distribution with a high energy tail and can be fitted by a κ distribution (Krimigis et al., 1983). Temperatures in the outer magnetosphere fell into the range from 16 to 21 keV during the Voyager 1 inbound pass and 35 to 45 keV for Voyager 2; somewhat lower temperatures were observed during the outbound passes. The high energy tail above 0.2 MeV follows a power law spectrum with $\gamma \sim 7$ (McDonald et al., 1980; Vogt et al., 1981). Near the equator, the diamagnetic pressure of this proton population constitutes a substantial fraction of the magnetic field pressure, and it appears that $\beta \sim 1$ when the pressure due to the low energy thermal plasma is added.

The proton pitch-angle distributions were pancake, and during the Pioneer 11 inbound pass, the distributions became progressively flatter from the magnetopause to $11.5 R_S$ but then became almost isotropic at $10 R_S$ (Bastian et al., 1980; McDonald et al., 1980). Superimposed on this pitch-angle distribution is the Compton-Getting effect which is a first order anisotropy due to the corotation of the plasma rest frame (Krimigis et al., 1981, 1982; Carbary et al., 1983; Thomsen et al., 1980). The magnitude of the first order anisotropy of the energetic particle population confirms that the plasma in the outer magnetosphere corotates nearly rigidly with Saturn out to $\sim 20 R_S$. The changes in the pitch-angle distribution (second order anisotropy) between the magnetopause and $11.5 R_S$ are qualitatively consistent with the inward diffusion and energization of protons starting at the magnetopause. The sudden disappearance of the anisotropy near $10 R_S$ would not be expected, and it is further surprising that this change in anisotropy was observed about $2 R_S$ closer to Saturn on the outbound pass of Pioneer 11. Again wave-particle interactions are the most likely cause because absorption by a dust ring,

which could cause a similar change of the angular distribution, should be symmetric between the noon and dawn directions.

A small flux of energetic ions heavier than protons are also found in the outer magnetosphere (Hamilton et al., 1983; Krimigis et al., 1981, 1982). The dominant species are H_2^+ and alpha particles (Fig. 18); Voyager 2 observed also a small flux of H_3^+ . The presence of molecular ions indicates an ionospheric source which could be either the ionosphere of Titan or Saturn; Hamilton et al. (1983) consider the latter the more likely source. Molecular ions are photodissociated with a lifetime that depends on the vibrational state of the molecule. The longest lifetime for H_2^+ ions is ~ 23 days, and this sets the time scale on which these ions have to be replenished. The spectrum of H_2^+ ions is very soft (Fig. 19) consistent with magnetospheric acceleration.

Ions from C, N, O through Fe are also found in the outer magnetosphere in the energy range from 0.2 to 0.4 MeV/nu. The composition of these ions and their relative abundances are consistent with a solar wind source (Fig. 18). From the composition of the magnetospheric plasma, ions accelerated from a local source should consist primarily of N^+ and O^+ with an almost complete absence of C. The abundance relative to He at equal energy per nucleon is also indicative of a solar wind source. Again the soft spectra (Fig. 19) indicate magnetospheric acceleration. These observations are most easily explained if the acceleration mechanism is sensitive to charge to mass ratio. The solar wind ions are more highly stripped and have a smaller charge to mass ratio than the ambient magnetospheric plasma (Hamilton et al., 1983).

Voyager 2 observed not only a much larger flux of heavy ions than Voyager 1 but also a proton to alpha ratio that is consistent with a solar wind source for the protons. In contrast, a local source for protons below ~ 1.5 MeV was

observed by both Pioneer 11 and Voyager 1 (Hamilton et al., 1983; McDonald et al. 1980; Simpson et al., 1980). At the Earth, solar wind plasma populates the plasma sheet of the magnetotail; at Saturn the dense local plasma population could populate the plasma sheet in the near tail but probably not the far tail with the boundary between the two populations moving in and out in response to interplanetary conditions. If the particle acceleration occurs primarily in the near tail region, one would normally expect to find a large excess of energetic protons and, occasionally under more disturbed conditions, a solar wind composition as existed during the Voyager 2 encounter.

The phase space density of energetic electrons and protons at constant magnetic moment or first adiabatic invariant is approximately independent of the L value in the outer magnetosphere provided their energy falls below the cut-off energy (Armstrong et al., 1983; Krimigis et al., 1981; McDonald et al., 1980; Van Allen et al., 1980). This is consistent with loss-free diffusion from a source near the magnetopause or distributed sources throughout the outer magnetosphere.

The Magnetotail

The outer magnetosphere in the pre-dawn direction at -90° to -120° from the subsolar direction differs substantially from the subsolar outer magnetosphere; the magnitude and direction of the magnetic field (Fig. 8) and the energetic particle population (Figs. 12 and 16) are distinct. Minor differences are already observable at $\sim 6 R_S$, and major differences start at $\sim 10 R_S$. The asymmetry relative to solar aspect is due to the onset of a magnetotail resembling its terrestrial counterpart. The most direct evidence for the magnetotail comes from Voyager 1 which passed through the tail lobe. The magnetic field observations have been modeled by a cross-tail current

(Fig. 20) which is driven by the convective electric field of the solar wind relative to the stationary magnetosphere (Behannon et al., 1981). This current passes through a plasma sheet located approximately in the magnetic equatorial plane near the planet and, further from the planet, in the X-Y plane of the solar-magnetospheric coordinate system. To simplify the model, the inclination of Saturn's magnetic axis relative to the ecliptic has been ignored in Fig. 20. The cross-tail current increases the radial component of the field which becomes almost parallel to the Saturn-Sun line. The tail presumably extends to a large distance from Saturn in the down stream solar wind; for instance, the Jovian magnetotail was observed at ~ 9 AU which is ~ 4 AU behind Jupiter (Scarf et al., 1981b, 1982; Lepping et al., 1982; Kurth et al., 1982; Desch, 1983.)

The radial component of the field reverses across the plasma sheet (Fig. 20). That such a reversal does occur can be seen by comparing the Voyager 1 data north of the plasma sheet with Voyager 2 observations south of it (Fig. 21). Only Pioneer 11 was at a low enough latitude ($\sim 4^\circ$) to see direct evidence for the existence of the plasma sheet. Because Saturn's magnetic axis is closely aligned with its spin axis, the position of the magnetic equator and plasma sheet does not wobble in latitude as is the case at Earth and Jupiter. Consequently, no plasma sheet crossings could be seen inside of $25 R_S$; however, near the magnetopause the solar wind can move the plasma sheet position to some extent and the sheet crossed Pioneer 11 several times as exemplified in Fig. 22.

Based on Voyager 1 data, the magnetotail diameter is $\sim 40 R_S$ at $25 R_S$ behind Saturn with a typical field of 3 nT. By matching the total magnetic flux content in the tail with that in the polar cap, one finds the boundary of the polar cap in the ionosphere between 75° and 78.5° (Ness et al., 1981).

Based on similar arguments, Smith et al. (1980) placed this boundary at $\sim 77^\circ$. Optical observations place the southern auroral zone between 78° and 81.5° (Sandel and Broadfoot, 1981).

Voyager 2 observed a stable tail field (Fig. 21) during the entire outbound pass; the field varied in a smooth fashion in both magnitude and direction. The Voyager 1 data, in contrast, indicated that the tail configuration changed noticeably during the outbound pass of that spacecraft (Behannon et al., 1981). The data in Fig. 21 suggest that the magnetopause may first have moved outward when Voyager 1 was at $\sim 13 R_S$. This caused a weakening of the tail field and a rotation towards the radial direction. Several hours later, in response to a compression, the field direction swung back to being nearly parallel to the model magnetopause surface (dashed curve in Fig. 21), and the field strength increased again. The greater average strength of the tail field is evident in the greater length of the Voyager 1 field vectors as compared to the Voyager 2 values (Fig. 21) even though Voyager 1 was at a greater distance down the tail.

There were no local simultaneous solar wind and interplanetary magnetic field observations; however, projections of the Voyager 2 interplanetary observations indicate that a temporary change in interplanetary field polarity and solar wind ram pressure may have occurred coincident with the changes observed while Voyager 1 was in the magnetotail (J.D. Sullivan and H.S. Bridge, private communications ; see Fig. 4 in Behannon et al., 1981). The interplanetary observations had to be projected over a distance of ~ 1.7 AU, but the good correspondence between variations seen by both spacecraft pre- and post-encounter increases our confidence in the validity of the procedure. A two order of magnitude decrease in the energetic particle flux accompanied this perturbation as if the field lines through the spacecraft

were suddenly connected to interplanetary field lines. (This is the dip at 10-15 R_S outbound, Figs. 12 and 16.) Simultaneously the thermal electron density (eV energy range) dropped to very low values and the electron temperature increased markedly. These observations demonstrate the large influence of interplanetary conditions on the magnetotail and probably also on the subsolar outer magnetosphere through coupling with the magnetotail.

Adjacent to the tail magnetopause Voyager 1 observed magnetic field and plasma behavior characteristic of "boundary layer" or "mantel" plasma flowing tailward (Behannon et al. 1983). A similarly directed flow is not evident in Voyager 2 outbound observations, possibly because of the very low pressure external to the magnetosphere when the observations were made.

A substantial population of 20-100 keV electrons and ions exist in the tail lobe at 20°-30° latitude (Figs. 12a and 16a); however, without data near the plasma sheet it is not known how their flux changes with latitude (Krimigis et al., 1981, 1982). The first order anisotropy of the ions reflects full or partial corotation superimposed on the solar wind convective electric field which drives the cross-tail current (Fig 23). The corotation velocity starts to fall below rigid corotation at $L \sim 27$ (Carbary et al., 1983). The anisotropy also has a field-aligned component which results from a net flow of energetic electrons and ions from the equator towards the ionosphere. As in the subsolar magnetosphere, electron pitch-angle distributions are field aligned. Fluxes of more energetic electrons and protons up to about 0.5 MeV are also found out to the magnetopause (Figs. 12 and 16b). These fluxes are subject to large temporal fluctuations. The electron flux disappears above 0.5 MeV. The ion flux above 0.5 MeV is due to cosmic rays that enter the magnetosphere (McDonald et al., 1980; Simpson et al., 1980; Vogt et al., 1981).

Just like the terrestrial and Jovian magnetotails, Saturn's tail is the site of particle acceleration. Below 100 keV, this results in a flow of particles towards the planet (Krimigis et al., 1981, 1982). At energies of ~ 0.4 MeV, ions were seen streaming away from Saturn by Voyager 1 between 35 and 45 R_S (Fig. 24a). Rather unusual bursts of electrons (Fig. 24b) accelerated to above 1 MeV were observed by Voyager 2 between 18 R_S and the magnetopause at $\sim 50 R_S$ (Vogt et al., 1982). For each burst the acceleration lasted about 5 min. with all energies (0.15 to > 1 MeV) peaking simultaneously and an energy dependent exponential decay with $\tau \sim 11$ min. for 1-2 MeV electrons and ~ 19 min. at ~ 0.4 MeV. Numerous acceleration mechanisms have been proposed to account for the observations in the Earth's tail, but the data at Saturn are still too fragmentary to identify specific mechanisms responsible for the observations.

The planetary field was found to be axisymmetric (see chapter on Magnetic Field Models), but the particle data indicate that an asymmetry may yet exist in the polar region. This is based on the apparent modulation of the < 0.5 MeV electron and ion spectra with approximately Saturn's period (Carbary and Krimigis, 1982). During the Voyager 2 outbound pass between 20 and 50 R_S about three modulation cycles were observed (Fig. 25) in the ratio of two electron channels [(22-35)/(183-500) keV], 10h 21m \pm 59m period, and of two ion channels [(43-80)/(137-215) keV], 9h 49m \pm 59m period. One cycle of modulation was observed by Voyager 1 in the same SLS longitude range of 0-90°. For a definition of the Saturn Longitude System (SLS) see Desch and Kaiser (1981).

Summary and Discussion

Saturn's outer magnetosphere looks superficially very much like the

Earth's. Both have a bow shock, magnetopause and magnetotail (Fig. 26), and substantial fluxes of energetic electrons and protons exist with soft spectra and large temporal variability. Acceleration of particles in the magnetotail is another common feature, and particle diffusion toward the planet with conservation of the first and second adiabatic invariants leads on the average to an increase in the particle flux above a fixed threshold energy. The size of both magnetospheres is controlled apparently by the pressure balance between the planetary magnetic field and dynamic ram pressure of the solar wind.

The most obvious differences between the two magnetospheres is the presence of thermal plasma out to the magnetopause at Saturn; in contrast, plasma is convected out of the terrestrial magnetosphere for $L > 6.5$. It appears that the β in the outer magnetosphere is ~ 1 ; this implies the possibility of plasma instabilities which may affect many properties of the outer magnetosphere. Specific instabilities have not been identified, but many as yet unexplained phenomena may or may not have such a cause. Among these are the energy dependent changes in the electron pitch-angle distribution (Fig. 14) and the almost regular changes in electron density and temperature observed between 10 and 15 R_S (Fig. 4). Plasma properties depend on solar aspect, which is consistent with the lack of symmetry of these phenomena between inbound and outbound passes.

Coincident minima in electron and ion densities were observed in the subsolar direction at the same dipole L values of 14 to 15 by Pioneer 11 and Voyagers 1,2 and at ~ 19 by both Voyagers (Lazarus et al., 1983); coincident decreases occurred also in the energetic particle population. Because of the large ring current, the dipole L value is only an approximate measure of the field-line distance at the equator, still the coincidence is surprising.

Lazarus et al. (1983) suggested the possibility of particulate or gaseous structure to explain the observations, but the lack of symmetry between inbound and outbound passes presents problems for this proposal. Other explanations are based on the escape of plasma bubbles, on occasional penetration of solar wind convection into the magnetosphere, or on the existence of a magnetospheric anomaly at a fixed Kronian longitude.

The frequent and large changes in the energetic particle fluxes (Figs. 12 and 16) have not been explained in detail. One possibility is that the shock which develops at boundaries between slow and fast solar streams disrupts the magnetosphere substantially more than the smoother transition observed at Earth. This change in the character of the solar wind and how it affects a magnetosphere deserves further study.

It appears that the magnetospheres of Earth, Jupiter, and Saturn have the same ratio between the energy content E_B of the planetary magnetic field and the energy content E of the particles trapped in the field (Connerney et al., 1983). In each case the ratio between the quiet time ring-current field ΔB at the equator and the equatorial planetary field B is $\Delta B/B \sim 1/2000$. According to the Dessler-Parker relation (Carovillano and Siscoe, 1973 and references therein):

$$E/E_B \sim 1.5 \Delta B/B(4)$$

The total energy content between the three magnetospheres varies by orders of magnitude and the energy sources driving the magnetospheres are quite different. Still the energy in the plasma and energetic particles builds up to only about 1/1000 of the field energy in each of the magnetospheres. It would appear that one or another plasma instability is triggered at that point to prevent further build up.

In summary, the three traversals of Saturn's magnetosphere have provided a good overall description, and as the analysis progresses, we will be able to fill in further details. However, our picture is bound to remain incomplete until long term observations are performed with a Saturn orbiter. In contrast to Jupiter, the solar wind appears to be the dominant energy sources and we need, therefore, observations of the magnetospheric response to various solar wind conditions.

Acknowledgements: The authors are greatly indebted to many scientists studying the magnetosphere of Saturn for helpful discussions, for prepublication copies of their work, and for permission to reproduce their illustrations. The help and support of the staff at the University of Arizona, especially Mrs. Mildred Mathews, is gratefully acknowledged.

REFERENCES

- Armstrong, T.P., M.T. Paonessa, E. V. Bell, II, and S.M. Krimigis, Voyager observations of Saturnian ion and electron phase space densities, J. Geophys. Res., Special Saturn Issue, 1983.
- Aubrey, M.P., M.G. Kivelson, and C.T. Russell, Motion and structure of the magnetosphere, J. Geophys. Res., 76, 1673-1696, 1971.
- Bastian, T.S., D.L. Chenette, and J.A. Simpson, Charged particle anisotropies in Saturn's magnetosphere, J. Geophys. Res., 85, 5763-5771, 1980.
- Behannon, K.W., J.E.P. Connerney, and N.F. Ness, Saturn's magnetic tail: Structure and dynamics, Nature, 292, 753-755, 1981.
- Behannon, K.W., R.P. Lepping, and N.F. Ness, Structure and dynamics of Saturn's outer magnetosphere and boundary regions, J. Geophys. Res., 88, Special Saturn Issue, 1983.
- Birmingham, T.J. and T.G. Northrop, Diffusion of cold magnetospheric ions, J. Geophys. Res., 86, 8971-8976, 1981.
- Brice, N.M., and G.A. Ioannidis, The magnetosphere of Jupiter and Earth, Icarus, 13, 173-183, 1970.
- Bridge, H.S., J.W. Belcher, A.J. Lazarus, S. Olbert, J.D. Sullivan, F. Bagenal, P.R. Gazis, R.E. Hartle, K.W. Ogilvie, J.D. Scudder, E.C. Sittler, A. Eviatar, G.L. Siscoe, C.K. Goertz, and V.M. Vasyliunas, Plasma observations near Saturn: Initial results from Voyager 1, Science, 212, 217-224, 1981.
- Bridge, H.S., F. Bagenal, J.W. Belcher, A.J. Lazarus, R.L. McNutt, J.D. Sullivan, P.R. Gazis, R.E. Hartle, K.W. Ogilvie, J.D. Scudder, E.C. Sittler, A. Eviatar, G.L. Siscoe, C.K. Goertz, and V.M. Vasyliunas, Plasma observations near Saturn: Initial results from Voyager 2, Science, 215, 563-570, 1982.
- Broadfoot, A.L., B.R. Sandel, D.E. Shemansky, J.B. Holberg, G.R. Smith, D.F. Strobel, J.C. McConnell, S. Kumar, D.M. Hunten, S.K. Atreya, T.M. Donahue, H.W. Moos, J.L. Bertaux, J.E. Blamont, R.B. Pophrey, and S. Linick, Extreme ultraviolet observations from Voyager 1 encounter with Saturn, Science, 212, 206-211, 1981.
- Carbary, J.F., and S.M. Krimigis, Charged particle periodicity in the Saturnian magnetosphere, Geophys. Res. Letter, 9, 1073-1076, 1982.
- Carbary, J.F., B. H. Mauk, and S.M. Krimigis, Corotation anisotropies in Saturn's magnetosphere, J. Geophys. Res., 88, Special Saturn Issue, 1983.
- Carovillano, R. L. and G. L. Siscoe, Energy and momentum theorems in magnetospheric processes, Rev. Geophys. Space Phys., 11, 289-353, 1973.
- Connerney, J.E.P., M.H. Acuña, and N. F. Ness, Saturn's magnetosphere, J. Geophys. Res., 88, Special Saturn Issue, Sept., 1983.
- Connerney, J.E.P., M.H. Acuña, and N. F. Ness, Saturn's ring current and inner magnetosphere, Nature, 292, 724-726, 1981.
- Desch, M.D., and M. L. Kaiser, Voyager measurement of the rotation period of Saturn's magnetic field, J. Geophys. Res., 8, 253-256, 1981.
- Desch, M.D., Radio emission signature of Saturn immersions in Jupiter's magnetic tail, J. Geophys. Res., 88, 6904-6910, 1983.
- Dessler, A. J. (Editor), Physics of the Jovian magnetosphere, Cambridge University Press, Cambridge, 1983.
- Eviatar, A., G.L. Siscoe, J.D. Scudder, E.C. Sittler, Jr., and J.D. Sullivan, The plumes of Titan, J. Geophys. Res., 87, 8091-8103, 1982.
- Eviatar, A., and M. Podolak, Titan's gas and plasma torus, J. Geophys. Res., 88, 833-840, 1983.
- Eviatar, A., R.L. McNutt, Jr., G.L. Siscoe, and J. D. Sullivan, Heavy ions in the outer Saturnian magnetosphere, J. Geophys. Res., 88, 823-831, 1983.
- Fälthammar, C.-G., Radial diffusion by violation of the third adiabatic invariant, in Earth's Particles and Fields, edited by B. M. McCormac, p. 157, Reinhold, New York 1968.

- Fillius, W., W.H. Ip, and C.E. McIlwain, Trapped radiation belts of Saturn: First look, Science, 207, 425-431, 1980.
- Frank, L.A., B.G. Burek, K.L. Ackerson, J.H. Wolfe, and J.D. Mihalov, Plasmas in Saturn's magnetosphere, J. Geophys. Res., 85, 5695-5708, 1980.
- Gurnett, D.A., F.L. Scarf and W.S. Kurth, The structure of Titan's wake from plasma wave observations, J. Geophys. Res., 87, 1395-1403, 1982.
- Goertz, C.K., Detached plasma in Saturn's front side magnetosphere, Geophys. Res. Lett., 10, 455-458, 1983.
- Hamilton, D.C., D.C. Brown, G. Gloeckler, and W.I. Axford, Energetic atomic and molecular ions in Saturn's magnetosphere, J. Geophys. Res., 88 Special Saturn Issue, 1983.
- Hartle, R.E., E.C. Sittler, Jr., K.W. Ogilvie, J.D. Scudder, A.J. Lazarus and S.K. Atreya, Titan's ion exosphere observed from Voyager 1, J. Geophys. Res., 87, 1383-1394, 1982.
- Hess, W.N., and G.D. Mead, editors, Introduction to space science, Gordon and Breach Science Publishers, 1968.
- Hess, W.N., The radiation belt and magnetosphere, Blaisdell Publishing Co., 1968.
- Hill, T.W., A. J. Dessler, and F. C. Michel, Configuration of the Jovian magnetosphere, Geophys. Res. Lett., 1, 3-6, 1974.
- Hill, T.W., Corotation lag in Jupiter's magnetosphere: Comparison of observations and theory, Science, 207, 301-302, 1980.
- Kennel, C.F., and F.V. Coroniti, Jupiter's magnetosphere in Solar System Plasma Physics - A Twentieth Anniversary Review, C.F. Kennel, L.J. Lanzerotti, and E.N. Parker eds., North-Holland Publishing Co., 1978.
- Krimigis, S.M., T.P. Armstrong, W.I. Axford, C.O. Bostrom, G. Gloeckler, E.P. Keath, L.J. Lanzerotti, J.F. Carbary, D.C. Hamilton, and E.C. Roelof, Low-energy charged particles in Saturn's magnetosphere: Results from Voyager 1, Science, 212, 225-231, 1981.
- Krimigis, S.M., T.P. Armstrong, W.I. Axford, C.O. Bostrom, G. Gloeckler, E.P. Keath, L.J. Lanzerotti, J.F. Carbary, D.C. Hamilton, and E.C. Roelof, Low-energy hot plasma and particles in Saturn's magnetosphere, Science, 215, 571-577, 1982.
- Krimigis, S.M., J.F. Carbary, E.P., Keath, T.P. Armstrong, L.J. Lanzerotti, and G. Gloeckler, General characteristics of hot plasma and energetic particles in the Saturnian magnetosphere: Results from the Voyager spacecraft, J. Geophys. Res., 88, Special Saturn Issue, 1983.
- Kurth, W.S., J.D. Sullivan, D.A. Gurnett, F.L. Scarf, H.S. Bridge, and E.C. Sittler, Observations of Jupiter's distant magnetotail and wake, J. Geophys. Res., 87, 10373-10383, 1982.
- Kurth, W.S., F.L. Scarf, D.A. Gurnett, and D.D. Barbosa, A survey of electrostatic waves in Saturn's magnetosphere, J. Geophys. Res., 88, Special Saturn Issue, 1983.
- Lanzerotti, L.J., C.G. MacLennan, R.P. Lepping, and S.M. Krimigis, On the plasma condition at the dayside magnetopause of Saturn, Submitted to Geophys. Res. Lett., 1983a
- Lanzerotti, L. J., C.G. MacLennan, W.L. Brown, R.E. Johnson, L.A. Barton, C.T. Reimann, J. W. Garrett, and J. W. Boring, Discussion of energetic ion erosion of the icy satellites of Saturn using Voyager data, J. Geophys. Res., 88, Special Saturn issue, 1983b.
- Lazarus, A., T. Hasegawa, and F. Bagenal, Long-lived particulate or gaseous structure in Saturn's outer magnetosphere?, Nature, 302, 230-232, 1983
- Lepping, R.P., and L.F. Burlaga, Geomagnetopause surface fluctuations observed by Voyager 1, J. Geophys. Res., 84, 7099-7106, 1979.
- Lepping, R.P., L.F. Burlaga, and L.W. Klein, Surface waves on Saturn's magnetopause, Nature, 292, 750-753, 1981a.

- Lepping, R.P., L.F. Burlaga, L.W. Klein, J.M. Jessen, and C.C. Goodrich, Observations of the magnetic field and plasma flow in Jupiter's magnetosheath, J. Geophys. Res., 86, 8141-8155, 1981b.
- Lepping, R.P., L.F. Burlaga, M.D. Desch, and L.W. Klein, Evidence for a distant ($> 8,700 R_J$) Jovian magnetotail, Geophys. Res. Lett., 9, 855-888, 1982.
- MacLennan, C.G., L.J. Lanzerotti, S.M. Krimigis, and R.P. Lepping, Low energy particles at the bow shock, magnetopause, and outer magnetosphere of Saturn, J. Geophys. Res. 88, Special Saturn Issue, 1983.
- McDonald, F.B., A.W. Schardt, and J.H. Trainor, If you've seen one magnetosphere, you haven't seen them all: Energetic particle observations in the Saturn magnetosphere, J. Geophys. Res., 85, 5813-5830, 1980.
- McIlwain, C.E., Coordinates for mapping the distribution of magnetically trapped particles J. Geophys. Res. 66, 3681-3691, 1961.
- McNutt, R.L., Jr., J.W. Belcher, and H.S. Bridge, Positive ion observations in the middle magnetosphere of Jupiter, J. Geophys. Res., 86, 8319-8342, 1981.
- Miura, A., and P.L. Pritchett, Nonlocal stability analysis of the MHD Kelvin-Helmholtz instability in a compressible plasma, J. Geophys. Res., 87, 7431-7444, 1982.
- Ness, N.F., The Earth's magnetotail, J. Geophys. Res., 70, 2989-3005, 1965.
- Ness, N.F., M.H. Acuña, R.P. Lepping, J.E.P. Connerney, K.W. Behannon, L.F. Burlaga, and F.M. Neubauer, Magnetic field studies by Voyager 1: Preliminary results at Saturn, Science, 212, 211-217, 1981.
- Ness, N.F., M.H. Acuña, K.W. Behannon, L.F. Burlaga, J.E.P. Connerney, R.P. Lepping, and F.M. Neubauer, Magnetic field studies by Voyager 2: Preliminary results at Saturn, Science, 215, 558-563, 1982.
- Northrop, T.G., The adiabatic motion of charged particles, Interscience Publishers, New York, 1963.
- Northrop, T.G., and T.J. Birmingham, Adiabatic charged particle motion in rapidly rotating magnetospheres, J. Geophys. Res., 87, 661-670, 1982.
- Pu, Z.Y., and M.G. Kivelson, Kelvin-Helmholtz instability at the magnetopause: Solution for compressible plasmas, J. Geophys. Res., 88, 841-852, 1983.
- Roederer, J.G., On the adiabatic motion of energetic particles in a model magnetosphere, J. Geophys. Res., 72, 981-992, 1967.
- Sandel, B.R., and A.L. Broadfoot, Morphology of Saturn's aurora, Nature, 292, 679-682, 1981.
- Scarf, F.L., The magnetospheres of Jupiter and Saturn, in The Magnetospheres of the Earth and Jupiter, ed., V. Formisano, D. Reidel Publishing Co., 443-449, 1975.
- Scarf, F.L., Possible traversals of Jupiter's distant magnetic tail by Voyager and by Saturn, J. Geophys. Res., 84, 4422-4424, 1979.
- Scarf, F.L., D.A. Gurnett, and W.S. Kurth, Plasma wave turbulence at planetary bow shocks, Nature, 292, 747-750, 1981a.
- Scarf, F.L., W.S. Kurth, D.A. Gurnett, H.S. Bridge, and J.D. Sullivan, Jupiter tail phenomena upstream from Saturn, Nature, 292, 585-586, 1981b.
- Scarf, F.L., D.A. Gurnett, W.S. Kurth, and P.L. Poynter, Voyager 2 plasma wave observations at Saturn, Science, 215, 587-594, 1982.
- Schulz, M., and L.J. Lanzerotti, Particle diffusion in the radiation belts, Springer, New York, 1974.
- Scudder, J.D., E.C. Sittler, Jr., and H.S. Bridge, A survey of the plasma electron environment of Jupiter: A View from Voyager, J. Geophys. Res., 86, 8157-8179, 1981.
- Simpson, J.A., T.S. Bastian, D.L. Chenette, R.B. McKibben, and K.R. Pyle, The trapped radiations of Saturn and their absorption by satellites and rings, J. Geophys. Res., 85, 5731-5762, 1980.

- Siscoe, G.L., L. Davis, Jr., P.J. Coleman, Jr., E.J. Smith, and D.E. Jones, Power spectra and discontinuities of the interplanetary magnetic field: Mariner 4, J. Geophys. Res., 73, 61-82, 1968.
- Siscoe, G.L., Magnetosphere of Saturn, in The Saturn System, D.M. Hunten and D. Morrison, editor, NASA Conference Publication 2068, 1978.
- Siscoe, G.L., Towards a comparative theory of magnetospheres, in Solar System Plasma Physics, Vol. III, eds. C.F. Kennel, L.J. Lanzerotti, and E.N. Parker, North-Holland Publishing Co., 1979.
- Siscoe, G.L., N.U. Crooker, and J.W. Belcher, Sunward flow in Jupiter's magnetosheath, Geophys. Res. Lett., 7, 25-28, 1980.
- Siscoe, G.L., and D. Summers, Centrifugally driven diffusion of ionogenic plasma, J. Geophys. Res., 86, 8471-8479, 1981.
- Sittler, E.C., Jr., K.W. Ogilvie, and J.D. Scudder, Survey of low energy plasma electrons in saturn's magnetosphere: Voyagers 1 and 2, J. Geophys. Res., 88, Special Saturn Issue, 1983.
- Slavin, J.A., E.J. Smith, P.R. Gazis, and J.D. Mihalov, A Pioneer-Voyager study of the solar wind interaction with Saturn, Geophys. Res. Lett., 10, 9-12, 1983.
- Smith, E.J., and J.H. Wolfe, Pioneer 10, 11 Observations of evolving solar wind streams and shocks beyond 1 AU, in Study of Traveling Interplanetary Phenomena 1977, M.A. Shea, D.F. Smart, and S.T. Wu editors, Reidel, Hingham, Mass., p.p. 227-257, 1977.
- Smith, E.J., L. Davis, Jr., D.E. Jones, P.J. Coleman, Jr., D.S. Colburn, P. Dyal, and C.P. Sonett, Saturn's magnetosphere and its interaction with the solar wind, J. Geophys. Res., 85, 5655-5674, 1980.
- Sonnerup, B.U.O., and L.J. Cahill, Magnetopause structure and attitude from Explorer 12 observations, J. Geophys. Res., 72, 171-183, 1967.
- Spreiter, J.R., A.L. Summers, and A.Y. Atksne, Hydromagnetic flow around the magnetosphere, Planet. Space Sci., 14, 223-253, 1966.
- Spreiter, J.R., A.Y. Atksne, and A.L. Summers, External aerodynamics of the magnetosphere, in Physics of the Magnetosphere, Editors R.L. Carovillano, J.F. McClay, and H.R. Radoski, D. Reidel Publ., Dordrecht, Holland, 1968.
- Stone, E.C., R.E. Vogt, F.B. McDonald, B.J. Teggarden, J. H. Trainor, J.R. Jokipii, and W.R. Webber, Cosmic ray investigation for the Voyager mission: Energetic particle studies in the outer heliosphere - and beyond, Space Sci. Rev., 21, 355-376, 1977.
- Strobel, D.F., and D.E. Shemansky, EUV emission from Titan's upper atmosphere. Voyager 1 encounter, J. Geophys. Res., 87, 1361-1368, 1982.
- Thomsen, M.F., T.G. Northrop, A.W. Schardt, and J.A. Van Allen, Corotation of Saturn's magnetosphere: Evidence from energetic proton anisotropies, J. Geophys. Res., 85, 5725-5730, 1980.
- Van Allen, J.A., B.A. Randall, and M.F. Thomsen, Sources and sinks of energetic electrons and protons in Saturn's magnetosphere, J. Geophys. Res., 85, 5679-5694, 1980.
- Vogt, R.E., D.L. Chenette, A.C. Cummings, T.L. Garrard, E.C. Stone, A.W. Schardt, J.H. Trainor, N. Lal, and F.B. McDonald, Energetic charged particles in Saturn's magnetosphere: Voyager 1 results, Science, 212, 231-234, 1981.
- Vogt, R.E., D.L. Chenette, A.C. Cummings, T.L. Garrard, E.C. Stone, A.W. Schardt, J.H. Trainor, N. Lal, and F.B. McDonald, Energetic charged particles in Saturn's magnetosphere: Voyager 2 results, Science, 215, 577-582, 1982.
- Warwick, J.W., D.R. Evans, J.H. Romig, J.K. Alexander, M.D. Desch, M.L. Kaiser, M. Aubier, Y. Leblanc, A. Lecacheux, and B.M. Pedersen, Planetary radio astronomy observations from Voyager 2 near Saturn, Science, 215, 582-587, 1982.
- Wolf, D.A., and F.M. Neubauer, Titan's highly variable plasma environment, J. Geophys. Res., 87, 881-886, 1982.
- Zwan, B.J. and R.A. Wolf, Depletion of plasma near a planetary boundary, J. Geophys. Res., 81, 1636-1648, 1976.

Table 1

Experiments in Saturn's Outer Magnetosphere

<u>Observations</u>	<u>S/C</u>	<u>Designator</u>	<u>Instrument</u>	<u>Principal Investigator</u>	<u>Institution</u>
Magnetic Field	Pioneer Pioneer Voyager	- - MAG	Vector Helium Magnetometer Flux Gate Magnetometer Double Triaxial Flux Gate Magnetometer	E.J. Smith M.H. Acuña N.F. Ness	JPL GSFC GSFC
Low Energy Plasma (0.1 - 8 keV)	Pioneer	-	Electrostatic Analyzer	J.H. Wolfe	ARC
Low Energy Charged Particles (20 - 500 keV)	Voyager Voyager	PLS LECP	Plasma Cup Counter Telescope Si Detector with Magnetic Particle Selection	H.S. Bridge S.M. Krimigis	MIT APL
Energetic Charged Particles (0.5 - 200 MeV)	Pioneer	-	Shielded GM Counters Si Detector	J.A. Van Allen	U. Iowa
	Pioneer	-	Counter Telescope Shielded Si Detector Fission Cell	J.A. Simpon	U. Chicago
	Pioneer	-	Cerenkov Counter Solid State Detectors	R.W. Fillius	UCD
	Pioneer	-	Counter Telescopes	F.B. McDonald	GSFC
	Voyager	CRS	Counter Telescopes	R.E. Vogt	CIT
	Voyager	LECP	Shielded Detectors Counter Telescope	S.M. Krimigis	APL
Plasma Waves (10 Hz - 56 Hz)	Voyager	PWS	Radiometer, electric dipole antenna	F.L. Scarf	TRW

Table 2

Positions of Bowshock and Magnetopause Crossings

Distance in R_S (60,330 km) and direction of crossing**

<u>Inbound</u>	λ^+	δ^{++}	Distance in R_S (60,330 km) and direction of crossing**
A) Bow Shock			
Pioneer 11	-4°	5°	4.1+, 23.1-, 20.0+
Voyager 1	17°	2°	26.1+
Voyager 2	15°	15°	31.5+, 29.0-, 27.9+, 26.6-, 23.6+
B) Magnetopause			
Pioneer 11	-1°	5°	17.3+
Voyager 1	18°	1°	23.7+, 23.4-, 23.1+, 22.9-, 22.8+
Voyager 2	22°	17°	18.5+
<u>Outbound</u>			
A) Magnetopause			
Pioneer 11	-85°	5°	30.3-, 33.2+, 34.7*, 35.9-, 39.0+, 39.8-
Voyager 1	-140°	23°	42.7-, 43.4+, 45.7-, 46.4+, 46.7-
Voyager 2	-97°	-29°	~48.1-, 48.4+, 51*, 51.8-, 51.9+, 52.0-, 52.7+, ~56.7-, 57.9+, 58.5-, 64.8+, 65.0-, ~56.2+, 70.4-
B) Bow Shock			
Pioneer 11	-81°	5°	49.3-, 56.8+, 59.9-, ~63+, ~64.5-, 81.2+, 94.8-, ~95+, ~100-
Voyager 1	-139°	24°	77.4-
Voyager 2	-94°	-29°	77.5-, 77.7+, 77.8-, 79.5+, 83.4-, 86.2+, 87.0-

† Angle in the ecliptic plane relative to the Saturn-Sunline

++ Kronian latitude

** A boundary moving outward past the spacecraft is indicated by + and moving inward by -

* Probable multiple crossings

Figure Captions

- Fig.1a Meridional projections of the Pioneer 11, Voyager 1, and Voyager 2 trajectories.
- Fig.1b Saturn encounter trajectories in cylindrical coordinates. This representation gives the spacecraft position in the plane through the spacecraft and the Saturn-Sun line (X axis) with the distance from that line plotted to the left for Voyager 1 and to the right for Voyager 2. For Voyager 1, the model bow shock and magnetopause boundaries are given and Pioneer 11 followed a very similar trajectory; for Voyager 2, observed average inbound and outbound shock location plus model magnetopause shapes are shown (Ness et al., 1982). The outbound "early" positions are based on the average of the first 5 outbound crossings; the outbound "last" curve is based on the last crossing (Bridge et al., 1982) and preserves the earlier shape of the magnetopause (courtesy of Behannon et al., 1983).
- Fig.2 The magnetic field (9.6s averages) observed while Voyager 1 traversed the bow shock, magnetosheath and entered the magnetosphere of Saturn. Notice the absence of a systematic change in the field direction (λ and δ) at the bow shock and the major change in direction that occurred at the magnetopause. The semi-periodic changes in the field intensity in the magnetosheath are anticorrelated with the electron density. The angles λ and δ are expressed in a heliographic, spacecraft-centered coordinate system, such that $\lambda = \tan^{-1} B_T/B_R$ and $\delta = \sin^{-1} B_N/B$. The Vector R is radially away from the Sun; T is parallel to the the Sun's equatorial plane, normal to R and positive in the direction of Saturn's orbital motion; and $N = R \times T$ is within 2° of being normal to the ecliptic plane. The day numbers in the trajectory insert refer to spacecraft positions at the start of the referenced day (courtesy of Lepping et al., 1981a).
- Fig.3 Sketch of magnetopause surface wave observed during the inbound pass of Voyager 1. The X_{MP} axis is aligned with the unperturbed magnetopause, and the Voyager 1 trajectory is shown relative to the "tailward" moving wave. D_3 , D_4 , and D_5 refer to the 3rd, 4th, and 5th magnetopause crossing and the change in the width of the line indicates variability of the estimated magnetopause thickness (courtesy of Lepping et al., 1981a).
- Fig.4 Electron densities and temperatures observed during the inbound pass of Voyager 1. The high density and low temperature regions numbered 1 to 4 have been attributed to a plasma plume from Titan, with number 1 corresponding to the most recent interaction and number 4 to an interaction which occurred 3 Saturn periods earlier. The low density region between $L = 18$ and 19 corresponded to an almost complete disappearance of the thermal plasma (adopted from Sittler et al., 1983).

- Fig.5 Models of the electron density in Saturn's magnetosphere inferred from Voyagers 1, 2 (Bridge et al., 1982) compared with the ion densities derived from Pioneer 11 plasma ion data (Frank et al., 1980). Also shown is the ion density computed from the ring current model of Saturn's magnetic field (Connerney et al., 1983). The locations of the orbits of Enceladus, Thethys, Dione, and Rhea are indicated by arrows labeled E, T, D and R (courtesy of Connerney et al., 1983)
- Fig.6 A high resolution spectrum of positive ions obtained by the thermal plasma cup on Voyager 1 during the inbound pass at $L \sim 15$. Although the heavy ion peak has been fitted with a curve corresponding to O^+ , an equally acceptable fit is obtained for N^+ (courtesy of Bridge et al., 1981).
- Fig.7 Relative plasma distribution functions between 14 and 18 R_S observed during the inbound passes of Voyagers 1 and 2 at Kronian latitudes of -2° and $+18^\circ$, respectively. The distribution functions were derived from low resolution mode spectra of the side-looking plasma cup (D sensor). Peaks appearing at a low energy per charge (10-100 volts) are attributed to H^+ and those at high values (> 800 volts) are attributed to N^+ . Note the high temperature of the H^+ ions at the latitude of Voyager 2 (18°) and the near absence of N^+ ions (courtesy of Bridge et al., 1982).
- Fig.8 Comparison of the magnetic field strength observed by Voyager 1 with pure dipole and dipole plus ring current models. The Voyager 1 trajectory, illustrated below the observations, shows the distance from the equatorial plane. Note the different scale used for the vertical spacecraft position (courtesy of Connerney et al., 1981).
- Fig.9 Projection of the Voyagers 1 and 2 hourly average magnetic field vectors into the noon-midnight meridian plane (X-Z plane in solar-magnetospheric coordinates, see Ness, 1965). Intersection of the plane with a cylindrically symmetric magnetopause are also shown. During the Voyager 1 inbound pass, the magnetosphere was initially more compressed and then more dynamic when the spacecraft was between 10 and 15 R_S (courtesy of Behannon et al., 1983).
- Fig.10 The top panel displays the proton energy density ϵ_p computed for protons with energies above 40 keV as a function of radial distance. Any heavy ion admixture would increase the energy density. The middle panel shows the magnetic-field energy density ϵ_M based on in-situ observations (Ness et al., 1981). The bottom panel shows β also under the assumption that the ions were O^+ rather than H^+ . Data from the inbound pass are shown with a solid line and outbound data with a dotted line (courtesy of Krimigis et al., 1983).
- Fig.11 Differential energy spectra for ions (upper panel) and electrons (lower panel) observed by Voyager 2. The last inbound bow shock and magnetopause crossings are indicated by BS and MP, respectively. Because of the high radiation background, spectra are not shown near closest approach (courtesy of Krimigis et al., 1982).

- Fig.12 Energetic electron intensities observed during the Voyager 1 pass. The upper panel shows 15m averages observed with the LECP experiment (courtesy of Krimigis, 1983). The lower panel shows Voyager 1 data in heavy lines with curves 1, 2, 4, and 6 corresponding to electron energies of 0.15 to 0.4 MeV, > 0.35 MeV, > 0.60 MeV, and > 2.6 MeV, respectively. Curves 3 and 5 give Pioneer 11 rates for energies > 0.25 MeV and 2.0 MeV, respectively, normalized to the geometric factor of the Voyager instrument. The magnetopause crossings are indicated by MP with a circle around the MP for the Pioneer crossing (courtesy of Vogt et al., 1981).
- Fig.13 Polar histograms of sectorized electron counting rates (32-minute average) observed with Pioneer 11. The dashed circle gives the spin average rate. The dashed arrow shows the projection of the magnetic field into the scan plane, and the dashed line gives the direction of the second order anisotropy (courtesy of McDonald et al., 1980).
- Fig.14 Thirty-two minute averages of second-order anisotropies of electrons in three energy intervals as observed with Pioneer 11. The pitch-angle distribution represented by this term corresponds to $1 + b \sin^2 \theta$, where $b = 2A_2/(1-A_2)$. Pancake (perpendicular to the field) distributions result from $A_2 > 0$ and dumbbell (field-aligned) distributions from $A_2 < 0$. No corrections have been made for the inclination of the magnetic field relative to the scan plane. The positions of Saturn's satellites are indicated by arrows (courtesy of McDonald et al., 1980).
- Fig.15 A 1.8-second average frequency spectrum of wide-band data observed by Voyager 1 inbound at $L = 15.6$ and a latitude of -2.3° . This emission is spread over a substantial frequency range and is therefore not due to the usual narrowband Langmuir waves (courtesy of Kurth et al., 1983).
- Fig.16 Energetic ion intensities observed by Voyager 1. The ions consist primarily of protons; the two highest energy rates in the lower panel responded only to protons. The upper panel shows 15m averages observed with the LECP experiment (courtesy of Krimigis, 1983) and the lower panel shows 1h average fluxes observed with the CRS experiment.
- Fig.17 Typical differential proton spectra in the outer magnetosphere and magnetotail observed by Voyager 1. The indicated dipole L values correspond to the position at the middle of the 1 hour averaging interval. The open circles represent LECP data and the crosses CRS data.
- Fig.18 Mass histograms of light and heavier ion species in the subsolar outer magnetosphere. The histograms were derived from 2-dimensional pulse-height matrices accumulated over 10h periods by Voyagers 1 and 2. Note the nearly equal abundance of H_2 molecules and He ions. The flux of medium weight nuclei was much higher during the Voyager 2 flyby. A histogram of energetic solar ions is shown for comparison by a dashed line in panel (d). The relative lack of nitrogen suggests solar wind origin rather than the plasma torus in the outer magnetosphere (courtesy of Hamilton et al., 1983).

- Fig.19 Energy spectra of the most abundant ion species averaged over the same 10h period as Fig. 18. A single power law in energy fits the H, He, and Voyager 1 C + N + O data. The H₂ spectrum (open circles) and Voyager 2 C + N + O spectrum (triangles) requires 2 components with a cutoff above 0.4 MeV which falls at least as fast as E⁻⁸. The H₃ ions were observed over such a narrow energy range that no spectrum could be derived. Interplanetary intensities and spectra of H, He, and C + N + O observed just prior to encounter are shown with dashed lines (courtesy of Hamilton et al., 1983).
- Fig.20 Model of Saturn's magnetic field in the noon-midnight meridian plane (solar magnetospheric coordinates). The model is based on a centered dipole planetary field, an azimuthal ring current between 8-16 R_S (stippled) and a cross-tail current extending from 16 to 100 R_S which closes on the magnetopause boundary. Field lines are drawn every 2° of invariant latitude, and the projections of the observed magnetic field vectors (Voyager 1 outbound) are shown. The insert illustrates the cross-tail current in the solar magnetospheric X-Y plane (courtesy of Behannon et al., 1981).
- Fig.21 Magnetic fields measured in Saturn's magnetotail and predawn magnetosphere by Voyagers 1 and 2 are shown in the plane through the spacecraft and the Saturn-Sun line (X axis). Hourly averaged field vectors have been rotated about the X axis into this plane and their length represents the field strength, scaled logarithmically. Greater temporal variations were observed during the Voyager 1 outbound pass than during the Voyager 2 pass. Because of the expanded magnetosphere during the Voyager 2 outbound pass, it observed significantly smaller field magnitudes than Voyager 1 even though the latter was at a greater distance down the tail (courtesy of Behannon et al., 1983).
- Fig.22 Multiple current sheet crossings observed by Pioneer 11 just after entering the magnetosphere for the second time, when the magnetopause moved past the spacecraft near dawn. The data are presented in a principal axis (PA) system determined by minimum variance analysis (Sonnerup and Cahill, 1967), which minimizes variation in the angle theta. Current sheet crossing were accompanied by a decrease in the field magnitude B (courtesy of Smith et al., 1980).
- Fig.23 Fifteen-minute averages of fluxes and anisotropy parameters of 43-80 keV ions from the out bound pass of Voyager 2. The parameters are derived from a fit of the form $j = a_0 [1 + a_1 \cos(\alpha - \alpha_1) + a_2 \cos 2(\alpha - \alpha_2)]$. The angles α_1 and α_2 are measured relative to the projection of the corotation direction into the scan plane. The standard deviation of the fit to the data is given by σ and the ratio σ/a_1 is a measure of the significance of a_1 . The results should be discounted when this ratio approaches 1. The plus symbols indicate the expected anisotropy parameters from rigid corotation for a convected κ distribution. "MP" denotes magnetopause position while "M" indicates spacecraft maneuvers. The dipole L-shell position is given on top of the figure (courtesy of Carbary et al., 1983)

- Fig.24 The top panel shows tailward-streaming bursts of > 0.43 MeV protons. These were observed by Voyager 1 primarily near the magnetopause between 35 and $45 R_S$ (courtesy of Vogt et al., 1981). The lower panel shows electron counting rates in the dawn side outer magnetosphere observed with Voyager 2 at a latitude of -29° . Curve A displays the rate of 0.14 - 0.4 MeV electrons ($\times 10$); curve B, the rate of > 0.35 MeV electrons, curve C, the rate of > 0.6 MeV electrons; and curve D, the rate of 1 - 2 MeV electrons ($\times 0.1$). Typically, the electron fluxes increased by about an order of magnitude with a rise time of $\tau \sim 5$ min. The decay time was energy dependent with $\tau \sim 11$ min. above 1 MeV and ~ 20 min. at ~ 0.4 MeV (courtesy of Vogt et al., 1982).
- Fig.25 Ratios of counting rates (15 minute average) in two energy channels for electrons and ions. The dipole L shells of Rhea and Titan are shown as dotted lines, and the tick marks identify the minima used to determine the period. Times when the spacecraft was at an SLS longitude of 0° are indicated at the top of the figure (courtesy of Carbary and Krimigis, 1982).
- Fig.26 Schematic of the global structure of Saturn's magnetosphere. Bow shock and magnetopause positions are "typical". A two component H^+ - N^+ plasma fills the subsolar outer magnetosphere, with the heavier ion concentrated near the equator. Energetic proton pitch-angle distributions are pancake and electron distributions primarily dumbbell. An equatorial ring current extends into the outer magnetosphere and is continued by a plasma sheet in the magnetotail. Proton and electron acceleration occurs in the magnetotail. Streaming of low energy electrons and protons towards Saturn was observed in the tail lobes as well as streaming away from Saturn at higher proton energies. Major solar wind induced changes have been observed in the magnetic field properties, plasma densities and energetic particle fluxes.

ORIGINAL PAGE 19
OF POOR QUALITY

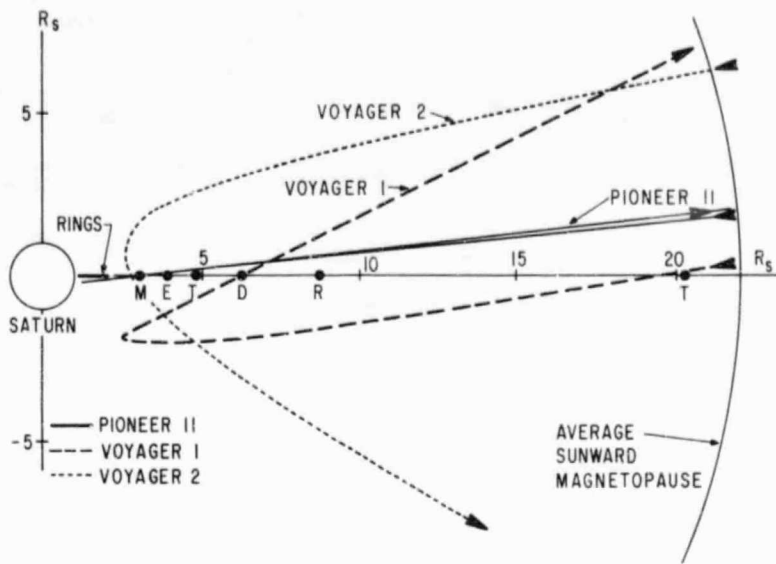


Figure 1a

VOYAGERS AT SATURN

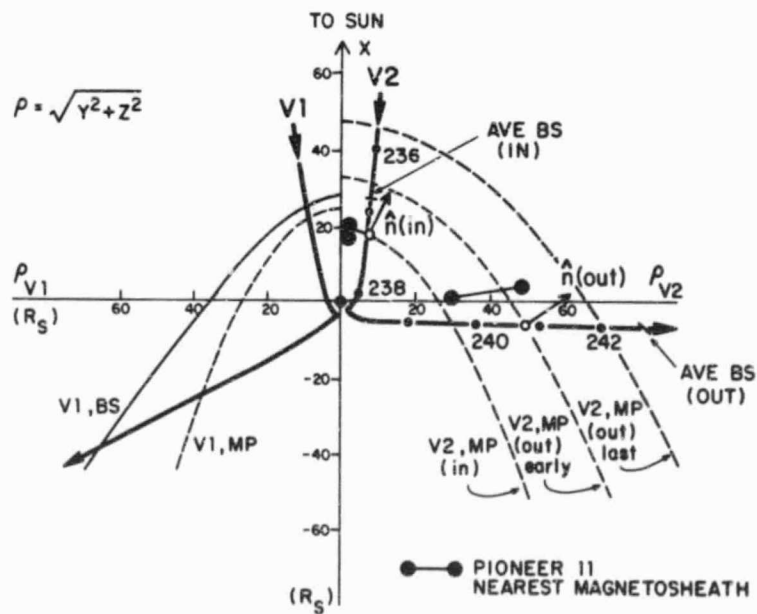


Figure 1b

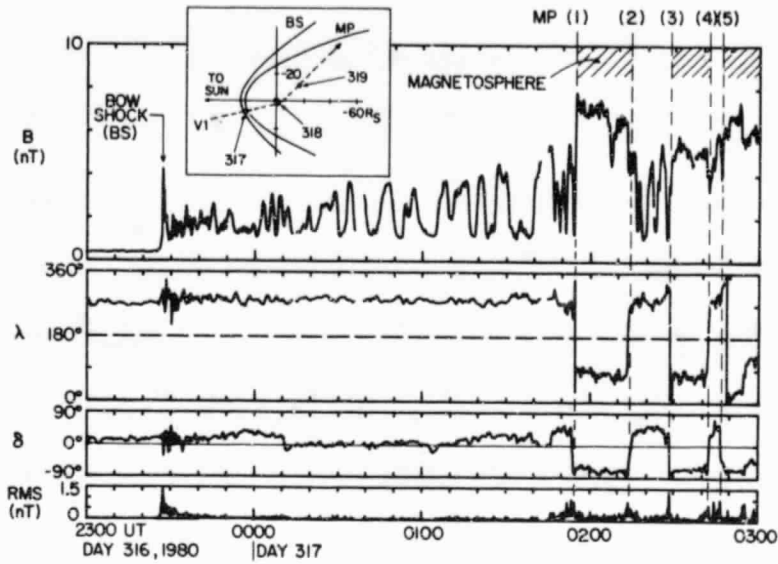


Figure 2

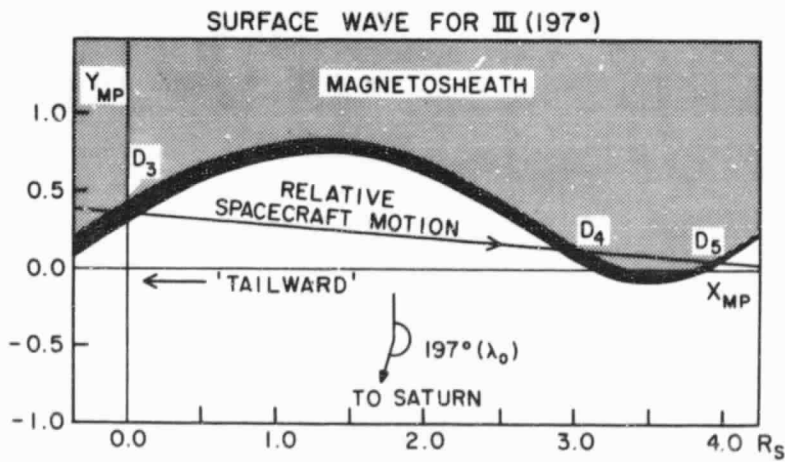


Figure 3

ORIGINAL PAGE IS
OF POOR QUALITY

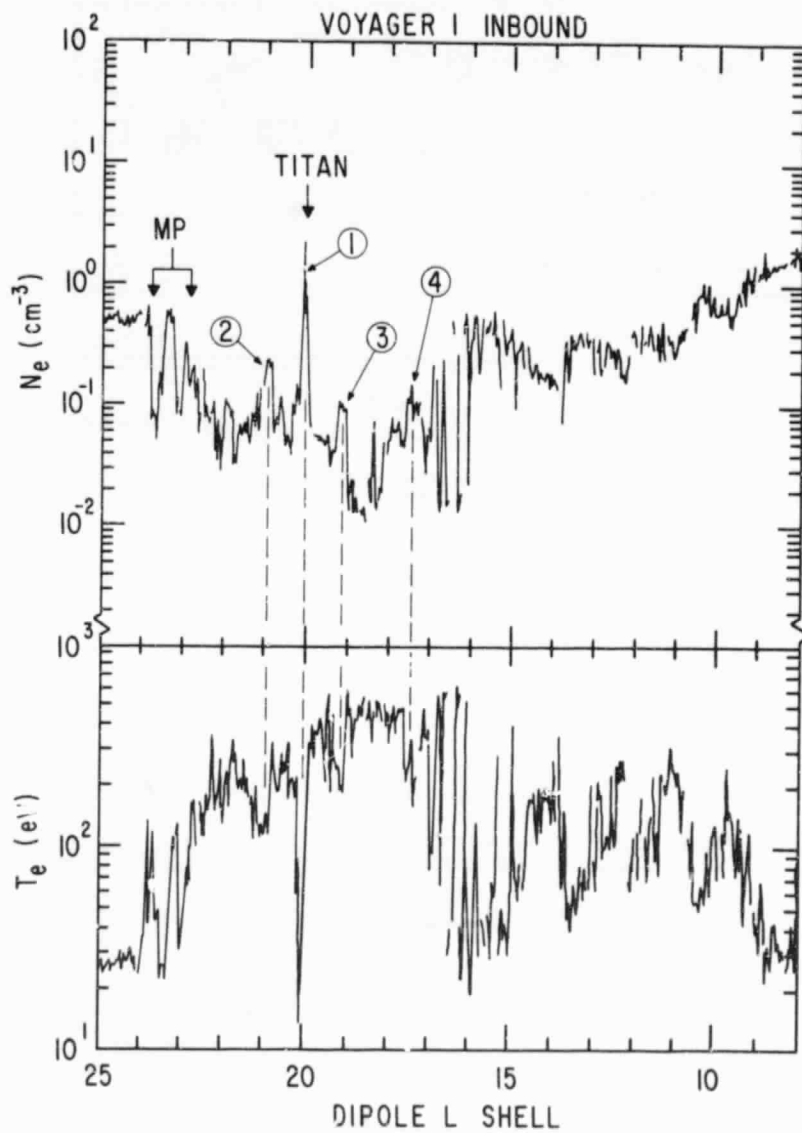


Figure 4

ORIGINAL PAGE IS
OF POOR QUALITY

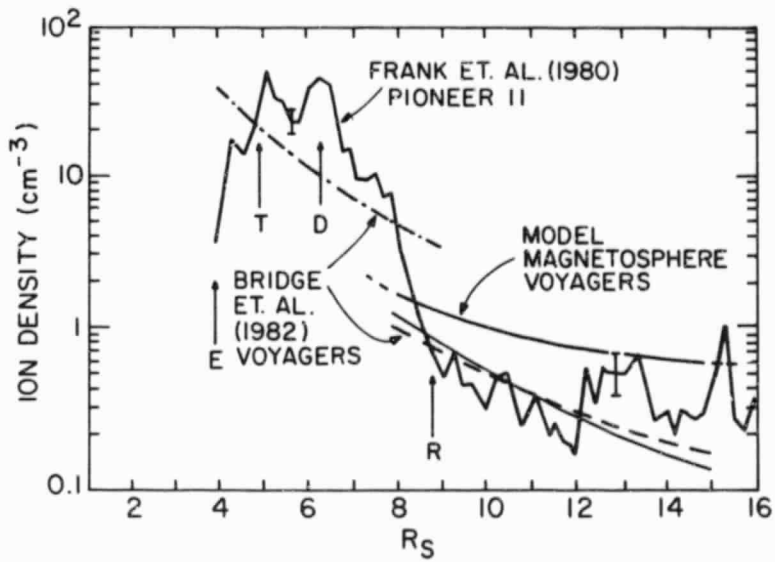


Figure 5

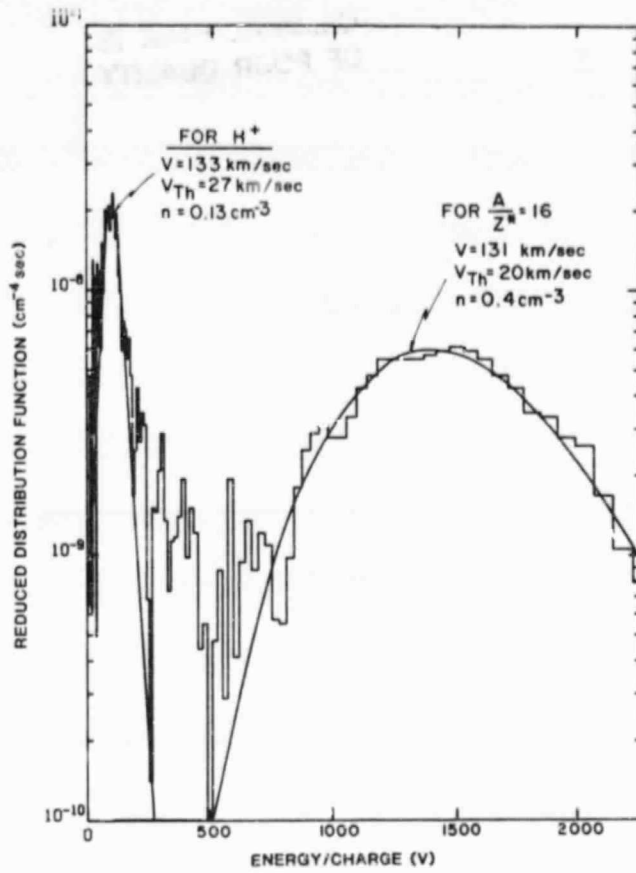


Figure 6

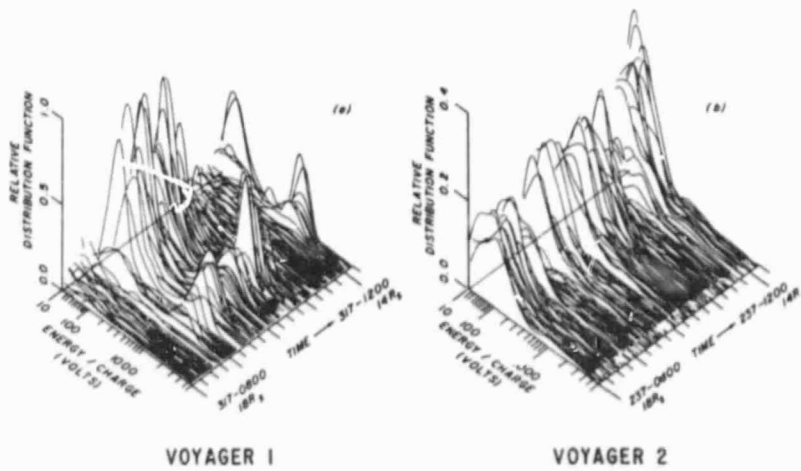


Figure 7

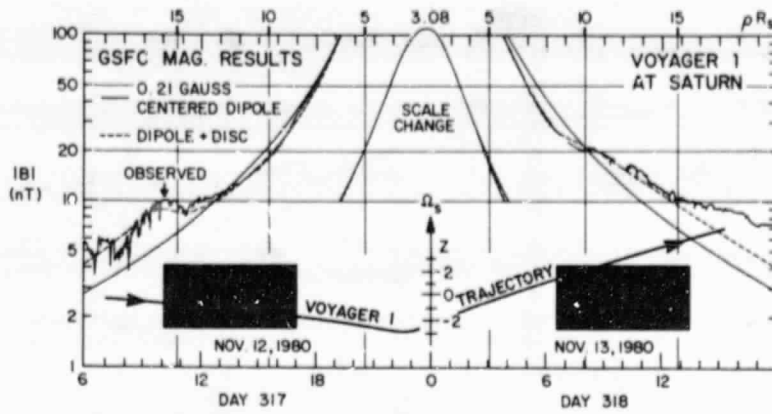


Figure 8

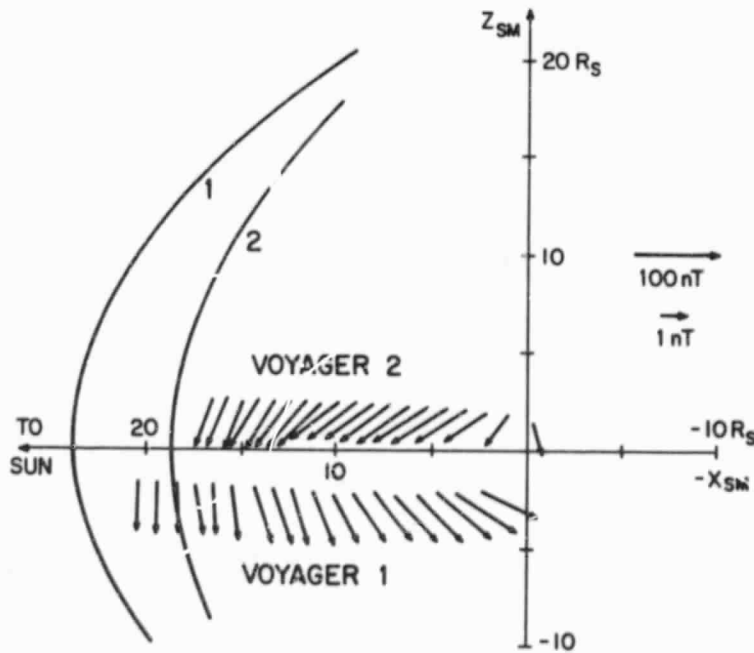


Figure 9

ORIGINAL PAGE IS
OF POOR QUALITY

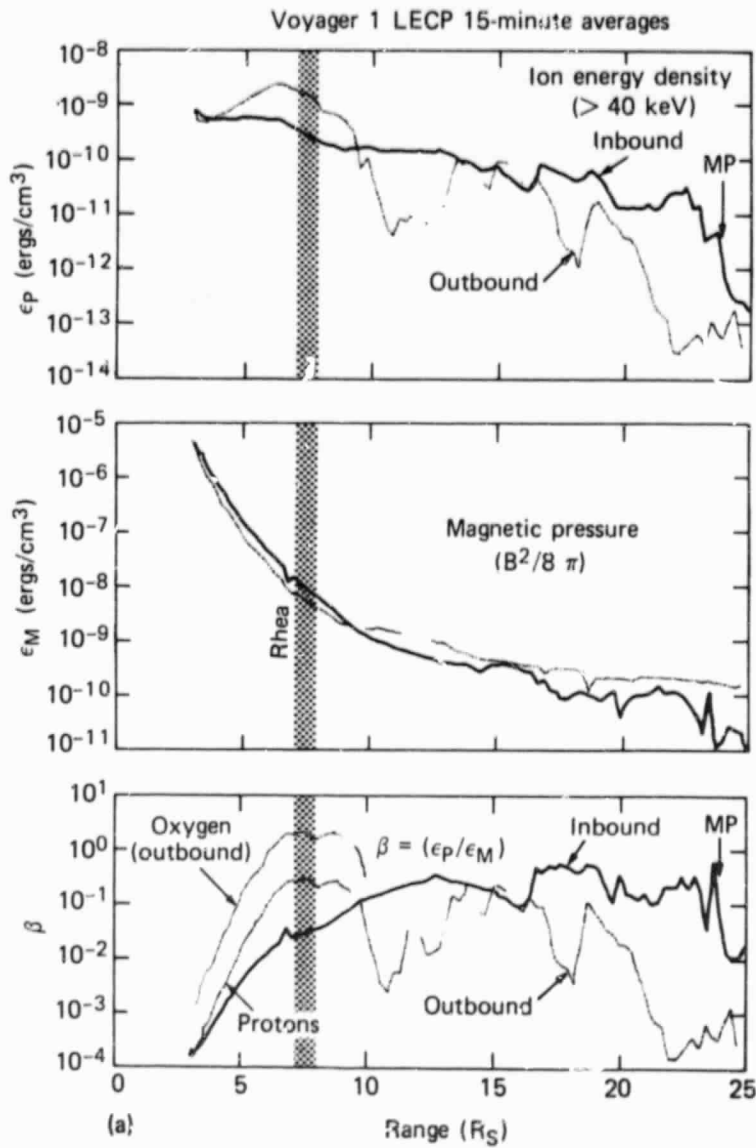


Figure 10

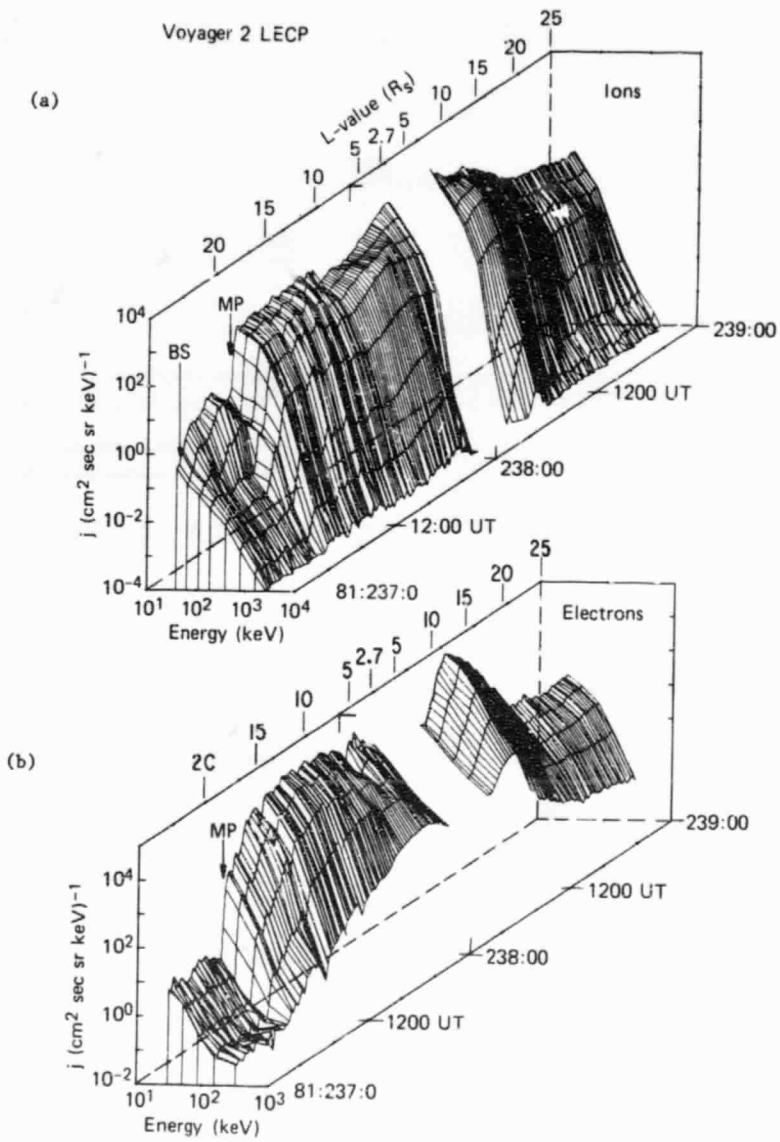


Figure 11

ORIGINAL PAGE IS
OF POOR QUALITY

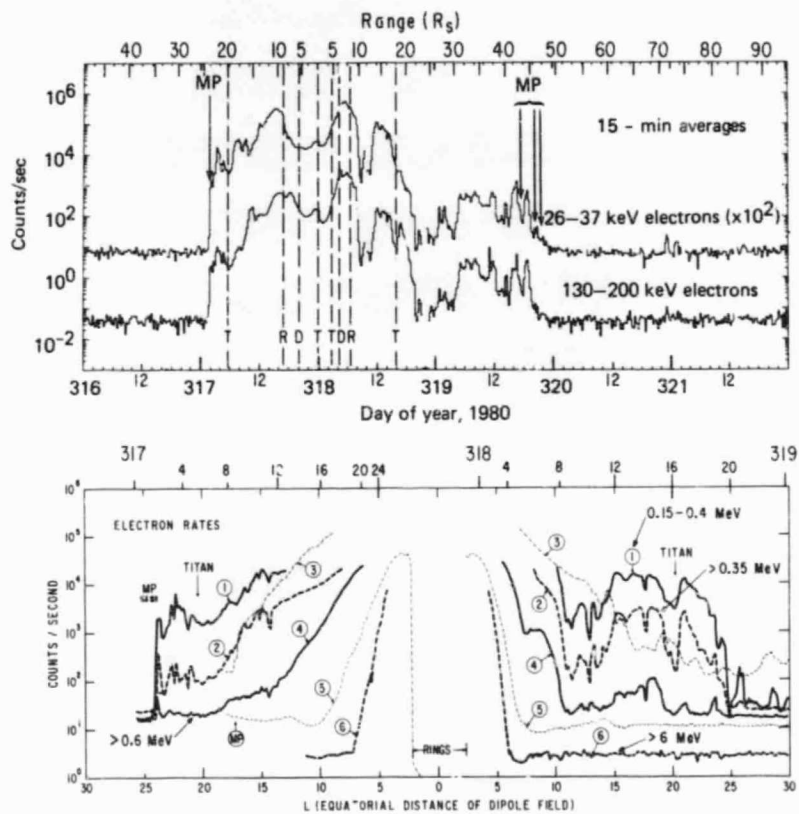
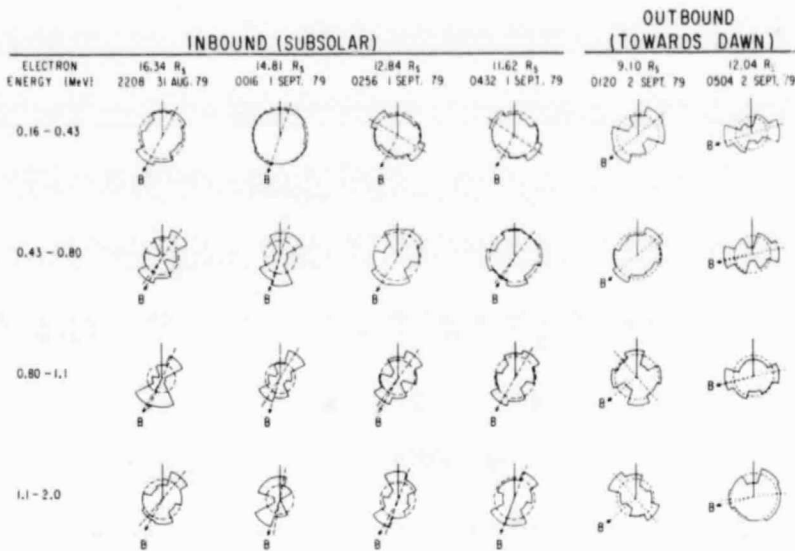


Figure 12



ORIGINAL PAGE IS
OF POOR QUALITY

Figure 13

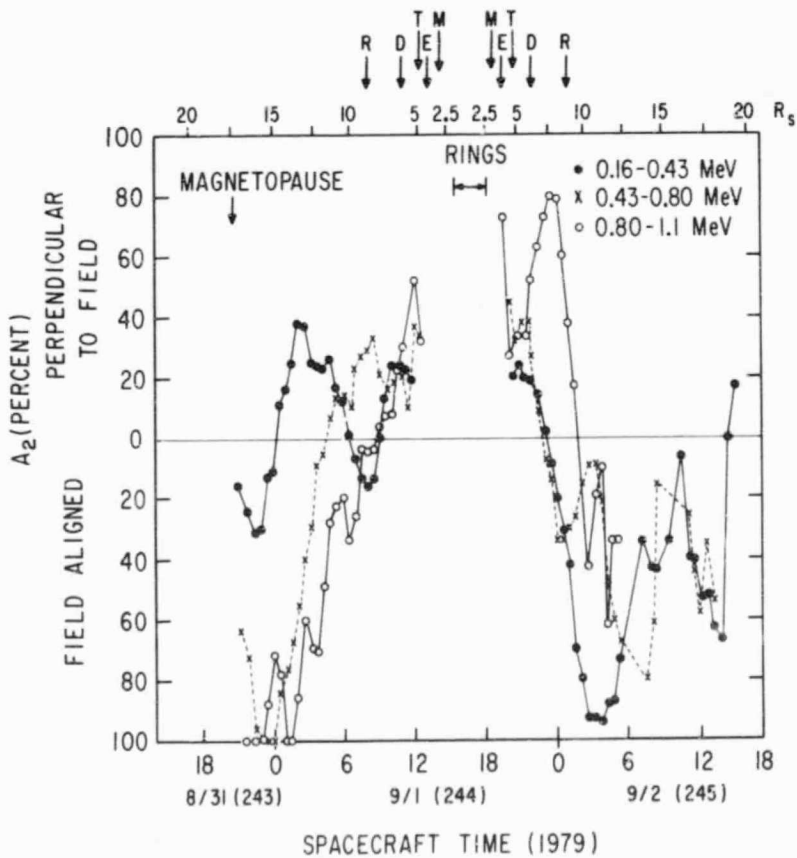


Figure 14

ORIGINAL PAGE IS
OF POOR QUALITY

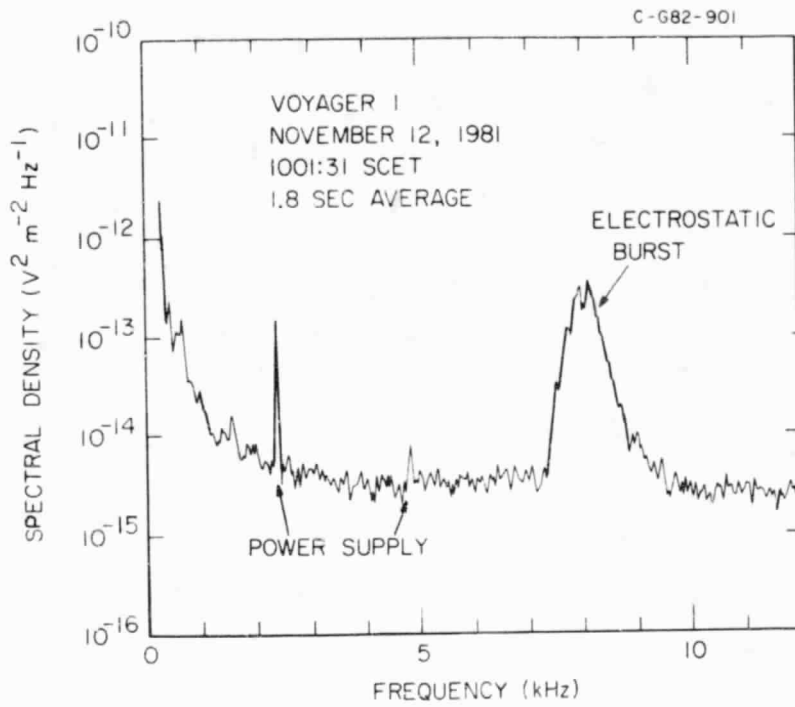


Figure 15

ORIGINAL PAGE IS
OF POOR QUALITY

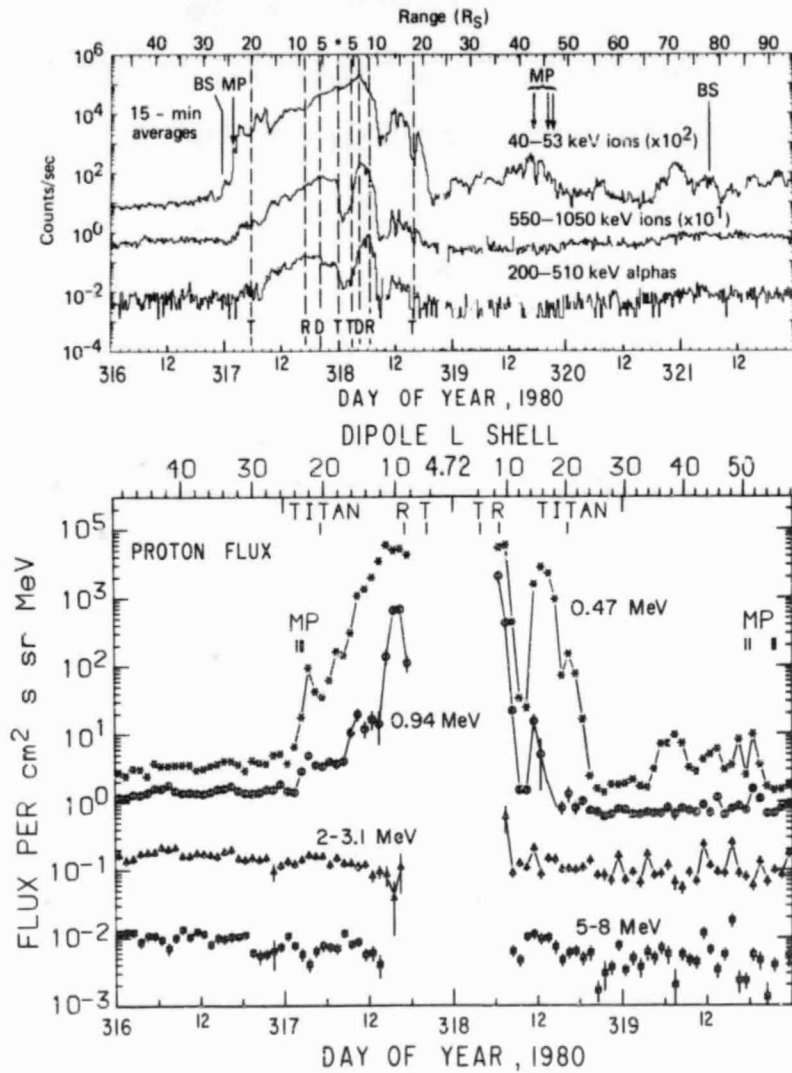


Figure 16

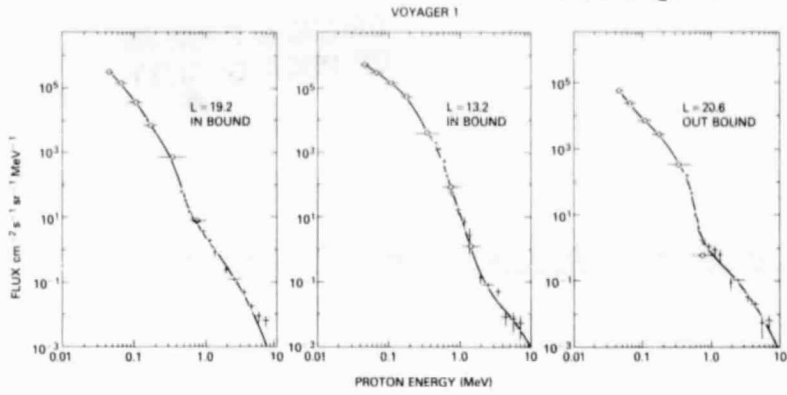


Figure 17

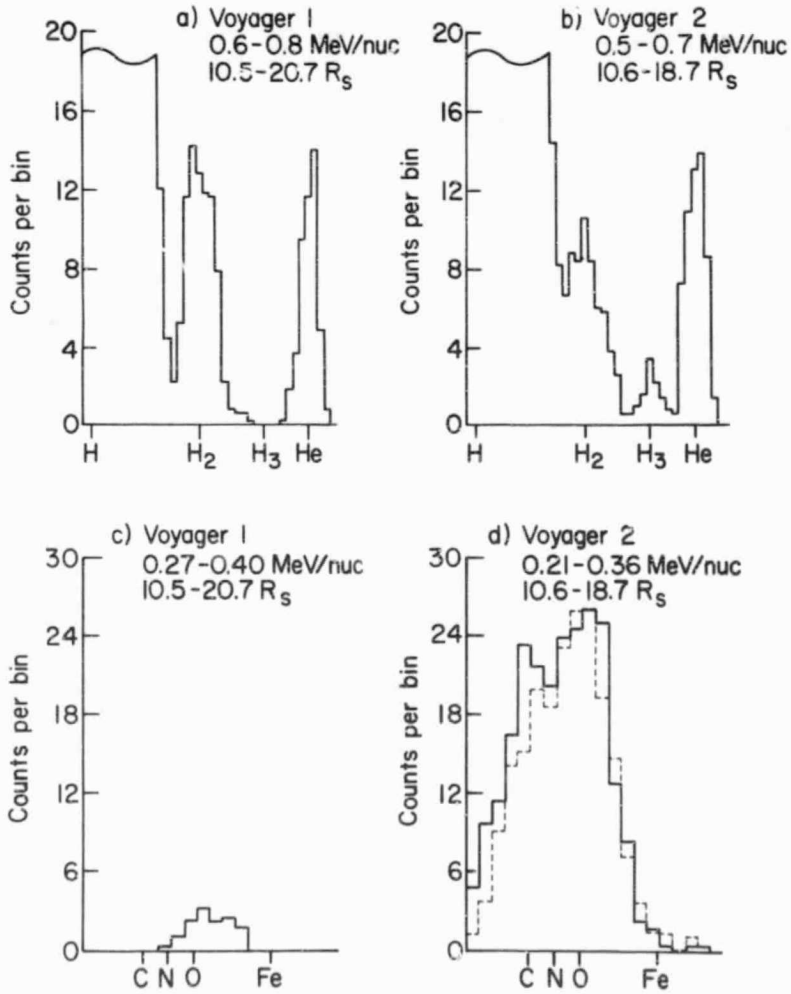


Figure 18

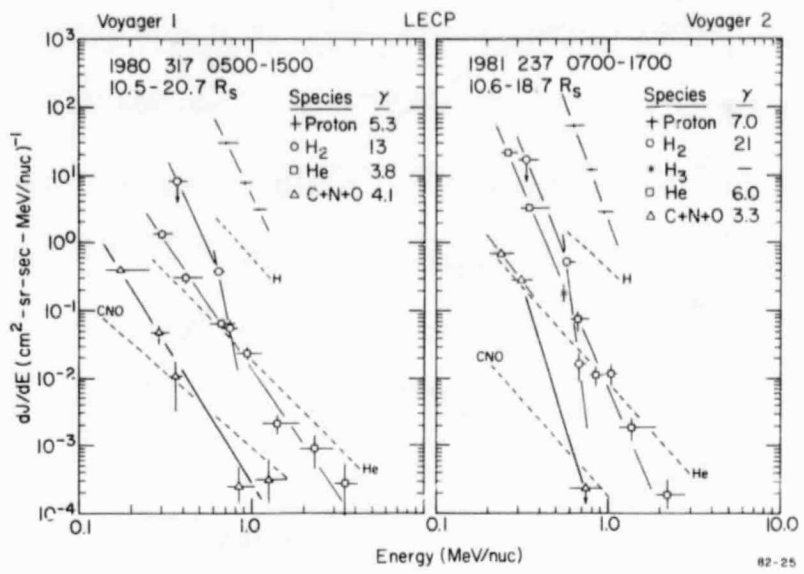


Figure 19

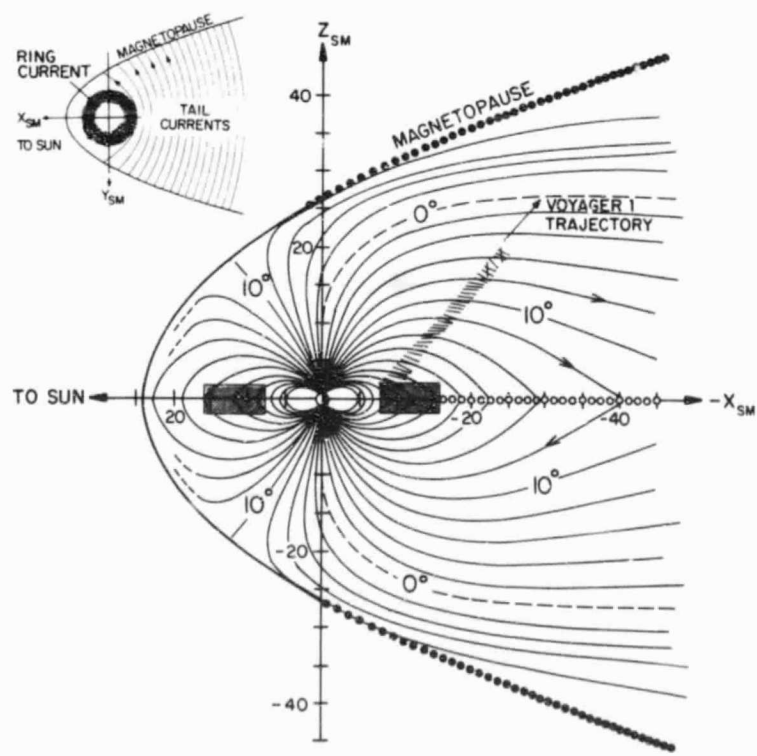


Figure 20

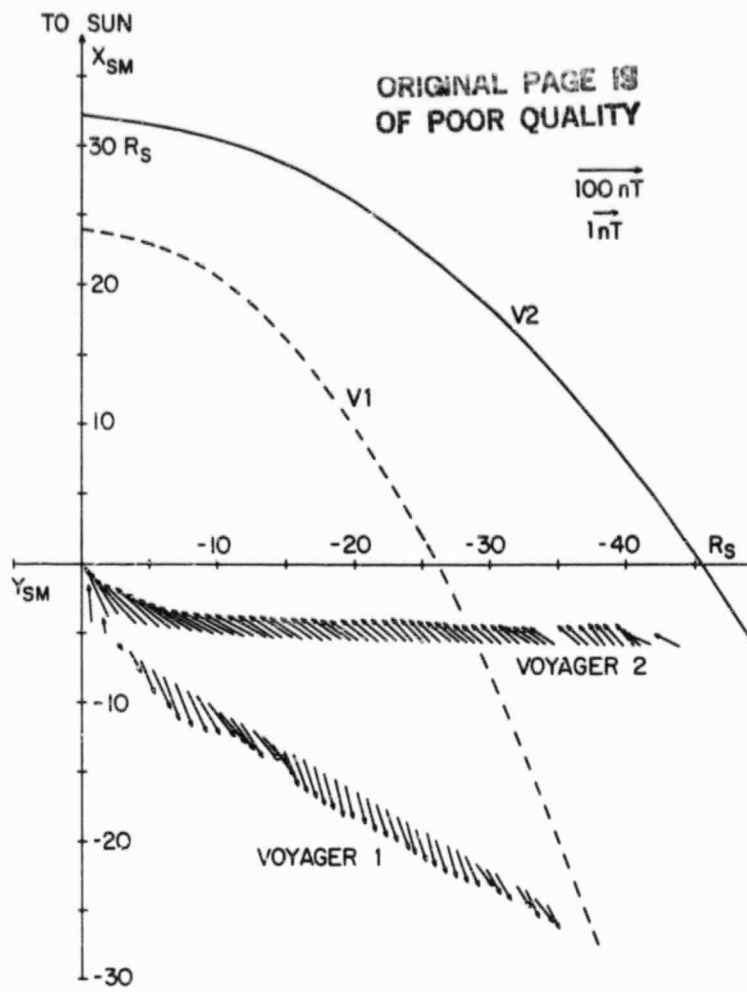


Figure 21

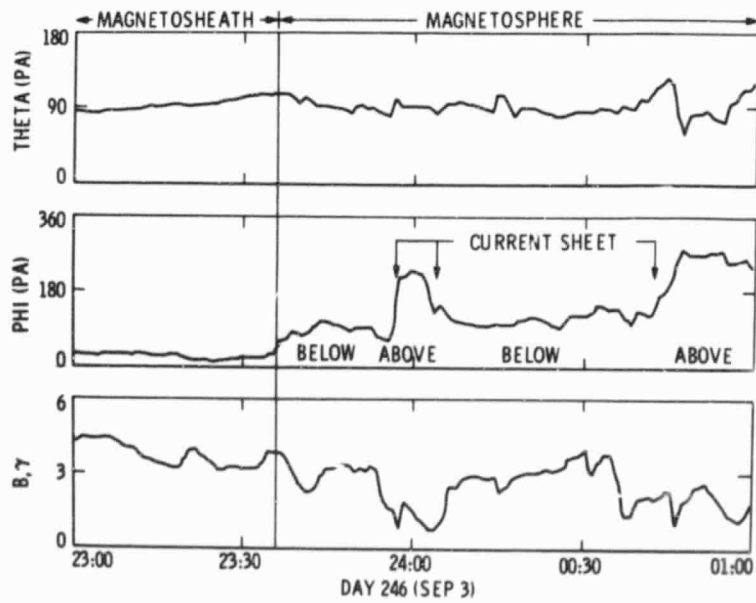


Figure 22

ORIGINAL PAGE IS
OF POOR QUALITY

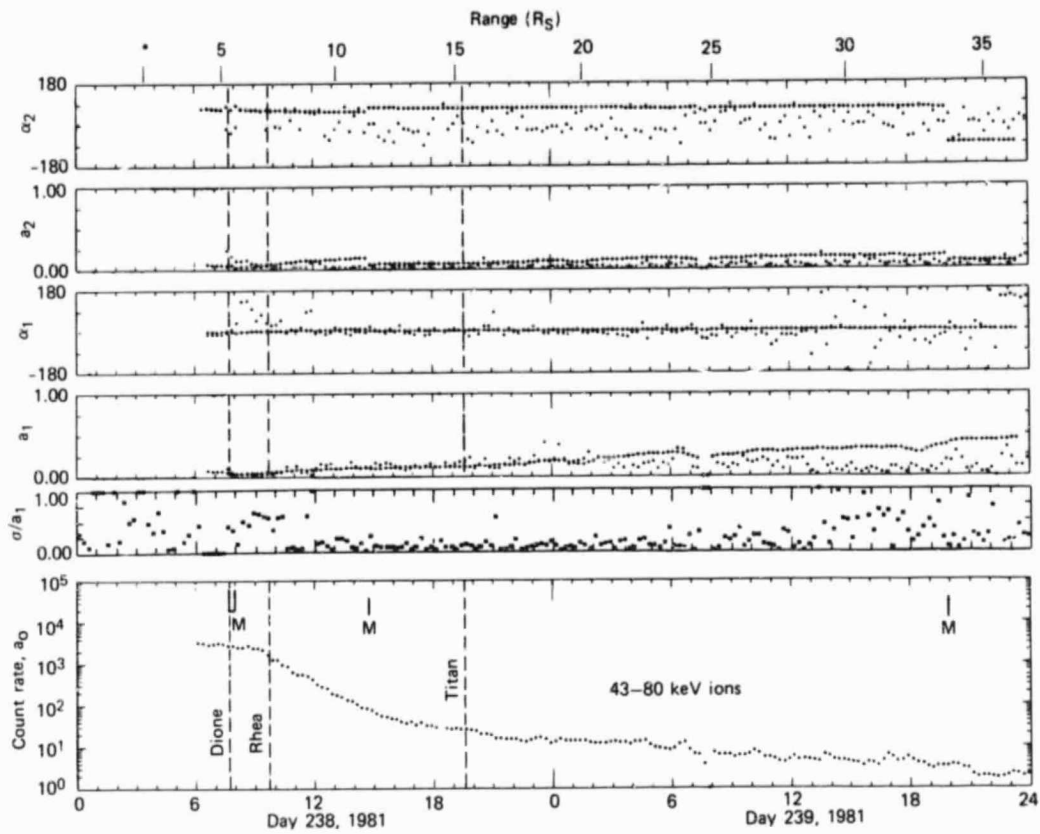


Figure 23

ORIGINAL PAGE IS
OF POOR QUALITY

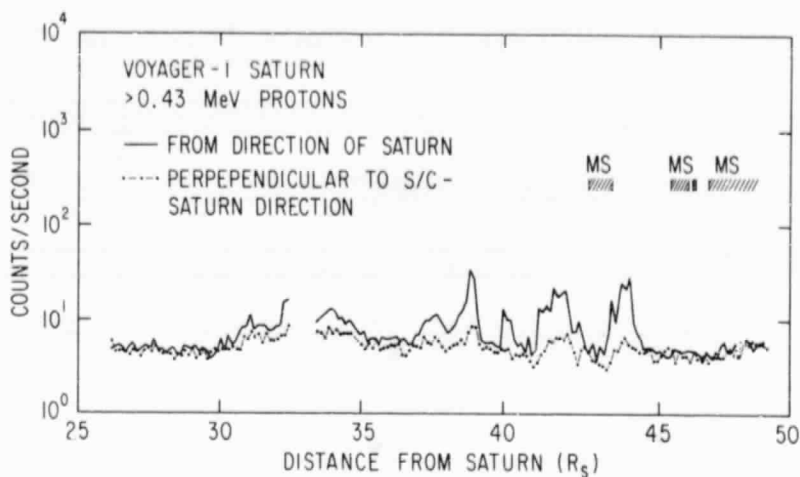


Figure 24 a

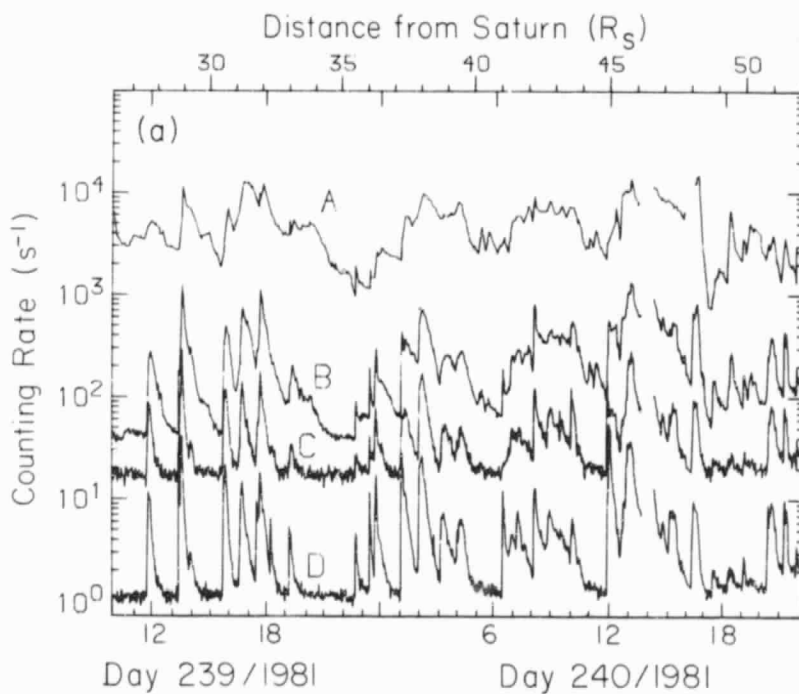


Figure 24 b

ORIGINAL PAGE IS
OF POOR QUALITY

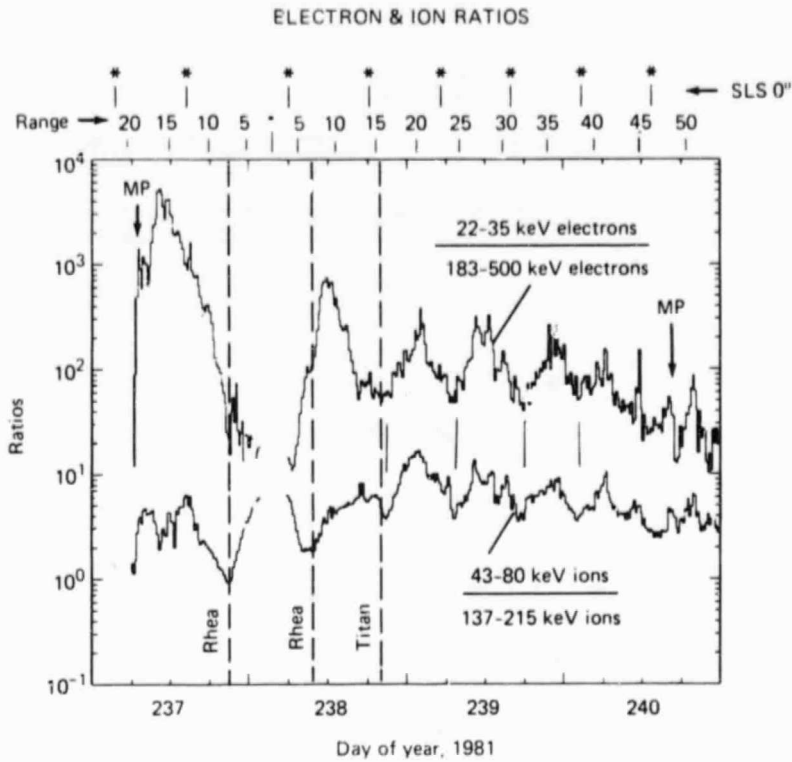


Figure 25

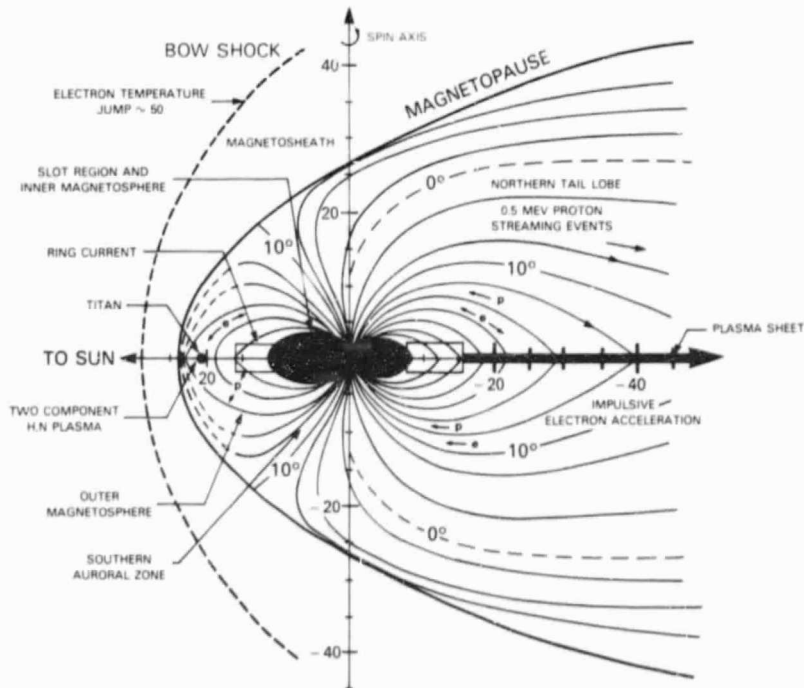


Figure 26